Naval Research Laboratory

Stennis Space Center, MS 39529-5004

NRL/FR/7322--04-10,070

Validation Test Report for the Simulating Waves Nearshore Model (SWAN): Cycle III, Version 40.11

Richard Allard
W. Erick Rogers
Ocean Dynamics and Prediction Branch
Oceanography Division

Suzanne N. Carroll
Kate V. Rushing
Planning Systems, Incorporated
Stennis Space Center 39529

September 2, 2004

REPORT DOCUMENTATION PAGE

Form Approved
OMB No. 0704-0188

1. REPORT DATE *(DD-MM-YYYY)*	2. REPORT TYPE	3. DATES COVERED *(From - To)*
02-09-2004	Formal Report	Final

4. TITLE AND SUBTITLE

Validation Test Report for the Simulating Waves Nearshore Model (SWAN) Cycle III, Version 40.11

5a. CONTRACT NUMBER

5b. GRANT NUMBER

5c. PROGRAM ELEMENT NUMBER

6. AUTHOR(S)

Richard Allard, W. Erick Rogers, Suzanne N. Carroll,* and Kate V. Rushing*

5d. PROJECT NUMBER

5e. TASK NUMBER

5f. WORK UNIT NUMBER

7. PERFORMING ORGANIZATION NAME(S) AND ADDRESS(ES)

Naval Research Laboratory
Oceanography Division
Stennis Space Center, MS 39529-5004

8. PERFORMING ORGANIZATION REPORT NUMBER

NRL/FR/7320--04-10,070

9. SPONSORING / MONITORING AGENCY NAME(S) AND ADDRESS(ES)

Office of Naval Research
800 N. Quincy St.
Arlington, VA 22217-5660

10. SPONSOR / MONITOR'S ACRONYM(S)

ONR

11. SPONSOR / MONITOR'S REPORT NUMBER(S)

12. DISTRIBUTION / AVAILABILITY STATEMENT

Approved for public release; distribution is unlimited.

13. SUPPLEMENTARY NOTES

*Planning Systems Incorporated, Stennis Space Center 39529
Submitted October 17, 2003.

14. ABSTRACT

The Simulating Waves Nearshore (SWAN) wave model represents a significant improvement for the U.S. Navy's nearshore wave modeling capability. SWAN is a full-plane model allowing wave propagation from any direction. Features include variable boundary conditions, multiple coordinate system options, refraction, wave-current interaction, nesting, and numerous output options. The OpenMP version of SWAN allows the model to be run on multiple processors on shared memory platforms, greatly reducing run times. This report validates SWAN version 40.11 with nine test cases that examine the wide-ranging features and modes through which the model can be operated.

15. SUBJECT TERMS

SWAN, Cycle III, 1-D version

16. SECURITY CLASSIFICATION OF:			17. LIMITATION OF ABSTRACT	18. NUMBER OF PAGES	19a. NAME OF RESPONSIBLE PERSON
a. REPORT	b. ABSTRACT	c. THIS PAGE			Rick Allard
Unclassified	Unclassified	Unclassified	UL	49	19b. TELEPHONE NUMBER *(include area code)* (228) 688-4894

Standard Form 298 (Rev. 8-98)
Prescribed by ANSI Std. Z39.18

CONTENTS

FIGURES

TABLES

VALIDATION TEST REPORT FOR THE SIMULATING WAVES NEARSHORE MODEL (SWAN): CYCLE III, VERSION 40.11

1. INTRODUCTION

The Office of Naval Research (ONR) is currently supporting applied research efforts to advance wave prediction. The ONR is working closely with the Naval Research Laboratory (NRL) to develop, integrate, and test wave prediction models. The long-term goal of this effort is to provide a commonly accepted third-generation wave model for shallow water for the purpose of basic research and operational wave computations. The objectives of the program include providing new capabilities to the Navy that allow for higher resolution modeling, incorporating currents, advancing wave measurement technology, and allowing for an improved interpretation of remotely sensed images of the sea surface. Participants in the program work in an open collaboration with other investigators and Department of Defense (DOD) laboratory and forecast center personnel.

2. MODEL DESCRIPTION

SWAN is a third-generation, phase-averaged model. Though applicable at any scale, it is most efficient when predicting wave conditions in small scale. It is capable of (but not limited to) the modeling of coastal regions with shallow water, (barrier) islands, tidal flats, local winds, and ambient currents. SWAN is based on the spectral action balance equation, treated in discrete form. Short-crested, random wave fields propagating simultaneously from widely varying directions can be accommodated. The SWAN model accounts for shoaling and refractive propagation (both depth and current induced), wave generation due to wind, energy dissipation due to whitecapping, bottom friction and depth-induced wave breaking, and nonlinear wave-wave interactions (quadruplets and triads), all through state-of-the-art formulations.

The use of unconditionally stable propagation schemes in SWAN averts excessive model run times in high-resolution applications. Near the coast, the SWAN model offers new capabilities to the Navy; for example, the simultaneous modeling of swell and wind sea propagating in any direction.

Efforts are underway to find a practical use for an existing, adjoint version of the model.

The 1-D mode of the model is similar to the 2-D mode, except there is not any variation (either in forcing/input or output) in the y-direction. In a typical case where x is the cross-shore direction, the slope is constant in the y-direction.

SWAN does not include diffraction. Thus, it is not appropriate for modeling scenarios in which there are large along-crest variations in the wave height over length scales similar to the waves themselves (for example, swell propagating past breakwaters into a harbor).

Manuscript approved September 30, 2003.

Cycle III of SWAN is stationary, optionally nonstationary, and formulated in Cartesian (small scale) or spherical (small and large scale) coordinates. The stationary mode is used only for waves with a relatively short residence time in the computational area under consideration. In other words, the travel time of the waves through the region is small compared to the time scale of the geophysical conditions such as wave boundary conditions, wind, tides, and storm surge. A quasistationary approach is used with stationary SWAN computations in a time-varying sequence of stationary conditions. A user can simplify SWAN by running in one-dimensional mode.

The SWAN model was developed at Delft University of Technology and continually undergoes improvements. SWAN is the most advanced wave model to date for coastal applications. Unlike most coastal wave models, SWAN is free and open-source, and has been described in the peer-reviewed literature. More than 250 institutions around the world currently use SWAN.

Perhaps the most favorable aspect of SWAN is its flexibility. The model has many options for input, solution, and output methods. Thus, knowledgeable users are able to set up very complex simulations with minimal effort. Modification of existing simulations (e.g., changing the computational resolution) is similarly trivial for the user.

The number of features and options of SWAN result in a relatively complex code. Also, the code is written by a large number of people over a long period of time. Thus, bugs are not uncommon. This is offset (to a large extent) by the wide usage of the code. Bugs are reported to a central location (Delft University and the two primary authors of SWAN) and most often quickly corrected.

2.1 Improvements Leading to SWAN 40.11

The first release of SWAN was Version 30.51. Since that time there have been three modified versions, the present working version (circa September 2003) being 40.11, which was released on October 27, 2000.

The second SWAN release (30.75) implemented the following modifications:

- SWAN is allowed to read and write wind and wave directions using both nautical and Cartesian conventions;
- Stationary boundary conditions can be imposed;
- SWAN produces a warning if computed significant wave height differs from the prescribed significant wave height at the up-wave boundary;
- SWAN will run in 1-D mode and optionally includes the effects of wave-induced setup.

The next release, Version 40.01, incorporated the following changes:

- SWAN is able to calculate wave-induced setup exactly for 1-D cases and approximately for 2-D cases;
- Introduction of nonstationary boundary conditions;
- The user now defines the initial conditions for stationary or nonstationary computations;
- SWAN has the ability to “hotstart” a run;
- SWAN also has the ability to combine stationary and nonstationary computations;
- The inspection of source terms at specified geographic points was introduced.

The following list summarizes the major changes and additions that were incorporated into Version 40.11:

- SWAN allows nesting in WAVEWATCH III;
- Spherical coordinates are available;
- The user can define obstacles at which waves are reflected;
- A higher order propagation scheme has been introduced for both the stationary and nonstationary modes.

Version 40.11 has been tested using improved benchmark tests.

2.2 The Future of SWAN

SWAN will be maintained by Delft University.

3. VALIDATION TEST DESCRIPTIONS AND RESULTS

The SWAN model (Version 40.01) was validated and verified successfully for a number of field (Ris et al. 1999) and academic cases. Field cases evaluate the model's ability to predict wave propagation and transformation in real situations. Academic cases isolate one or more specific physical phenomena. In these cases, waves are typically monochromatic and unidirectional, with comparison being made with analytical solutions. This validation was repeated (by Delft University) prior to the release of Version 40.11.

Validation of SWAN has been well documented. The SWAN test areas represent coastal regions where significant variability and sufficient data exist to accurately describe variability. The following test cases have been conducted for a variety of wind, current, and bathymetric conditions to compare the model's description of the evolution of 2-D wave energy spectrum against observational data. Table 1 assigns test numbers (for the purpose of this document only) and gives the location, date, and publication reference of each test.

For Field Tests 1 through 7, SWAN was used to generate computed data from different regions around the world. The computed data were compared to observational data of the same region to verify whether or not SWAN produced similar (accurate) results. For the academic tests (Tests 8 and 9), computed data generated by SWAN were compared to analytical solutions. **Note**: Field tests 1 through 5 were run using SWAN Version 40.01. However, Tests 1 through 3 were rerun using 40.11. This report preserves the 40.01 results since many of the referenced publications in this report used Version 40.01. Field tests 6 through 9 were run using SWAN Version 40.11.

3.1 Test 1: Haringvliet, the Netherlands

3.1.1 Purpose

Test 1 was conducted to verify SWAN Version 40.01 (in particular triads and regeneration of waves by local wind) in a complex bathymetry. A complete description of the test area, model setup, and comparison results can be found in Booij et al. (1999) and Ris et al. (1999).

Table 1 — Test Descriptions

Field Test	Location	Date	Longitude	Latitude	Reference
1	Haringvliet, Netherlands (SWAN 40.01, 40.11)	10/14/1982	3.8667° E	51.8667° N	Booij et al. 1999; Ris et al. 1999
2	Friesche Zeegat, Netherlands (SWAN 40.01, 40.11)	10/9/1992	6° E 10'	53° N 24'	Booij et al. 1999; Ris et al. 1999
3	Lake George, Australia (SWAN 40.01, 40.11)	4/1992-10/1993	149° E 08'	35° S 17'	Padilla-Hernandez and Monbaliu 2001
4	SandyDuck, North Carolina (SWAN 40.01)	9/22/1997-9/31/1997	74° 50'24"W 74° 28'18"W	36° 34'59"N 38° 30'12"N	Rogers et al. 2003
5	Lake Michigan (SWAN 40.01)	11/1995	86° 25'02"W 87° 01'12"W	45° 19'48"N 42° 40'12"N	Rogers et al. 2003
6	Mississippi Bight (SWAN 40.11)	11/01/2002-11/30/2002	90° W 87.5° W	29.0° N 30.8° N	Pers. Comm. Allard 2002
7	Oland, Sweden (SWAN 40.11)	3/1/2002-3/15/2002	16.68° E	56.1° N	Wakeham et al. 2002
Academic Test	**Test Phenomenon**	**Date**	**Longitude**	**Latitude**	**Reference**
8	Refraction (SWAN 40.11)	N/A	N/A	N/A	Mei 1983
9	Slanting Current (SWAN 40.11)	N/A	N/A	N/A	Hedges 1987; Jonsson 1993

3.1.2 Test Characteristics

Test 1 consisted of data analysis in the Haringvliet, a branch of the Rhine, on October 14, 1982 conducted by the Ministry of Transport, Public Works, and Water Management in the Netherlands. The area is a relatively shallow bay penetrating a few kilometers into the coast. There were no currents during the observations, as the sluices were closed and tides were low. The bay is partially protected from the southern North Sea by a shoal (the "Hinderplaat"), which extends across half of the bay entrance. The water depth (including water level) is 4 to 6 m with a surface area of 10 by 10 km. Figure 1 illustrates the bathymetry of the Haringvliet estuary and shows the locations of the observation stations. The waves approach the estuary from deep water and break over the shoal with a reduction of wave energy. Behind the shoal, the local wind regenerates the waves (which is evident as a high-frequency peak in the observed spectra). A constant and homogeneous wind speed U_{10} was considered for each test case. Currents were assumed to be absent.

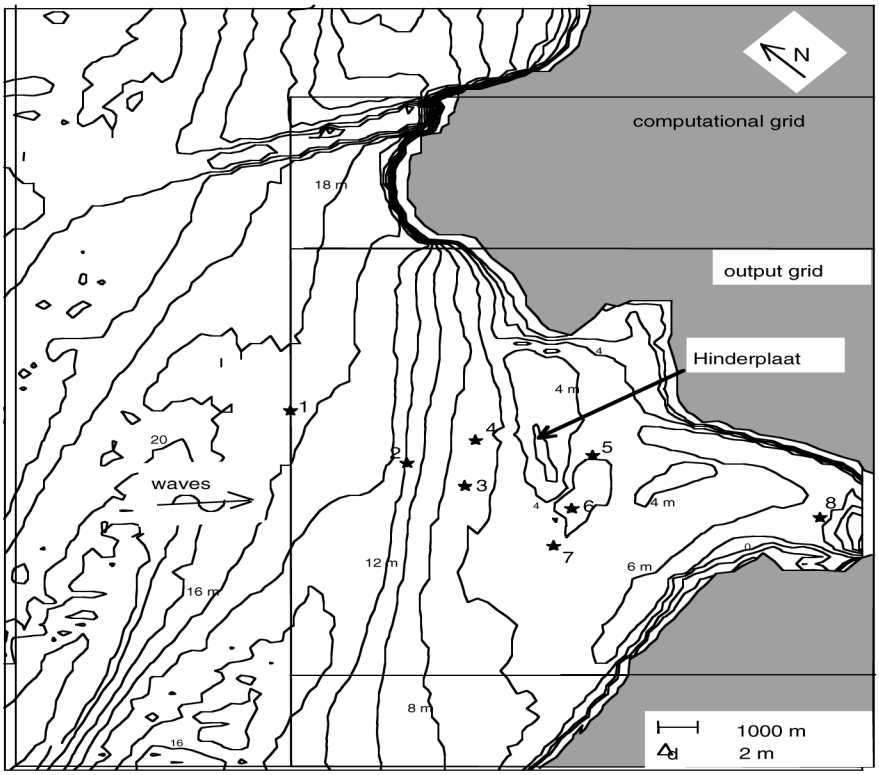

Fig. 1 — Bathymetry and station locations for Test 1

Test 1 compared the data computed by SWAN with the data taken from the Haringvliet buoy observations. The 2-D mode of SWAN was activated. SWAN simulations were performed at four different time levels, ranging from 21.00 to 24.00 hrs UTC, wind speeds ranging from 12 to 17 m/s, and water levels from 0.30 to 2.10 m. Test 1 was performed at these times and conditions because 1) the wind speed and direction were constant, 2) a storm event chosen had offshore wave heights exceeding 3 m, and 3) the water level was low enough to see the generation of a significant secondary peak in the spectra near the shoal but not so low that the shoal would be dry. The incident wave conditions and the wind speed and direction taken during the observations are given in Table 2. The size, range, and resolutions of the computational grids in geographic and spectral space, which were used in the computations of SWAN, are given in Table 3. All physical processes were activated in SWAN.

Table 2 — Wind and Incident Wave Conditions

Test Area	$H_{s,i}$ (m)	$T_{m01,i}$ (s)	$\theta_{\text{wave},i}$ (deg)	$\sigma_{\theta,i}$ (deg)	U_{10} (m/s)	θ_{wind} (deg)
Haringvliet	3.56	6.7	306	31	varies from 12-17	300-330

The variables are defined as $H_{s,i}$, incident significant wave height; $T_{m01,i}$, incident mean wave period; $\theta_{\text{wave},i}$, mean wave direction; $\sigma_{\theta,i}$, directional spreading; U_{10}, wind speed; and θ_{wind}, wind direction for the verification cases of this study.

Table 3 — Size, Range, and Resolution of the Computational Grids

Geographic Grid	
Size (km)	14.7 × 22.0
Resolution (m)	125 × 125
*Spectral Grid**	
Range in f (Hz)	0.052 to 1
Range in θ (deg)	0 to 360
Resolution	$\Delta f = 0.1f$, $\Delta\theta$ = 10 deg

Here f is spectra wave frequency; θ is spectral wave direction. * Above the maximum frequency, an f^{-4} tail is added to the spectrum.

The observed data were collected by one WAVEC pitch-and-roll buoy (Station 1), six Waverider buoys scattered around the shoal (Stations 2 to 7), and one wave gauge located about 5 km behind the shoal (Station 8). During the observations, the water depth over the shoal was 2 m. The wind velocity, wind direction, and water level were measured at a site near Station 6. The observations at the various stations were not synchronous; therefore, the two nearest observations on either side of 2300 UTC were considered at each station.

3.1.3 Results

Performance statistics are provided in Tables 4 and 5 for significant wave height and mean wave period, respectively. Comparisons between the wave buoys and SWAN 40.01 and the newer SWAN 40.11 model results are given in Fig. 2 for Test 1, Case 1. Figures 3 through 5 illustrate model/data comparisons for the remaining three cases for Test 1.

Table 4 — Performance of SWAN for Significant Wave Height H_s

$H_{s,i}$ (m)	H_s (m)	*Bias* (m)	*RMS* (m)	*SI*
3.56	1.85	0.23	0.33	0.18

Abbreviations are defined as $H_{s,i}$, incident significant wave height; H_s, mean observed significant wave height; and *SI*, scatter index.

Table 5 — Performance of SWAN for Mean Wave Period T_{m01}

$T_{m01,i}$ (s)	T_{m01} (s)	*Bias* (s)	*RMS* (s)	*SI*
6.7	5.3	-0.5	0.6	0.11

The incident mean wave period is T_{m01i}, the mean observed wave period is T_{m01}. *SI* is the scatter index.

The Scatter Index (SI) is used to quantify the performance of ocean wave models (Ris 1999). The *SI* is defined as the (RMS) error (RMSE) normalized with the average observed value:

$$SI = \frac{RMS_{error}}{\overline{X}},$$

where

$$RMS_{error} = \sqrt{\frac{1}{N}\sum_{N}(X_n - Y_n)^2},$$

where X_n represents the observed values, Y_n represents the computed values, N represents the number of observations, and $\overline{X}$ is the average observed value.

The pattern of the significant wave height as computed by SWAN was consistent with that of the observations. The significant wave height reduced gradually from the deepwater value of 3.6 to 2.5 m in front of the shoal and then very rapidly to about 0.7 m over the shoal. The mean wave period followed roughly the same pattern. A comparison of the observed significant wave height and mean wave period showed a reasonable agreement. However, the model slightly overestimated the significant wave height and underestimated the mean wave period.

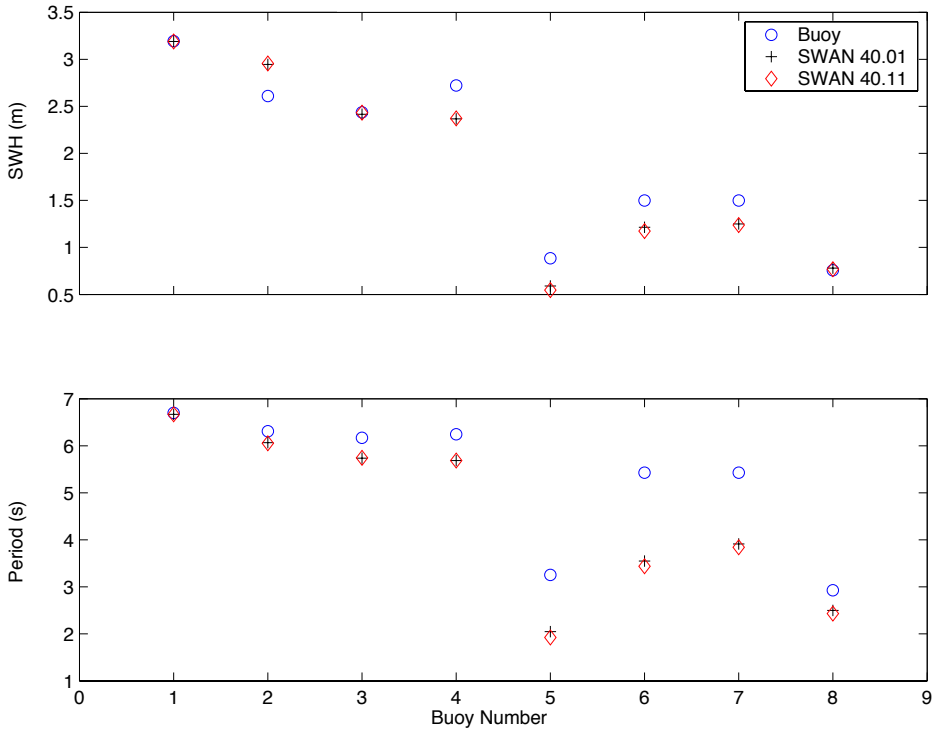

Fig. 2 — SWAN 40.01 and 40.11 output and buoy data comparisons for significant wave height and mean wave period for Test 1, Case 1, which represents wind speed and direction at 17 m/s and 330 deg on 10/14/82 at 21.00 h UTC

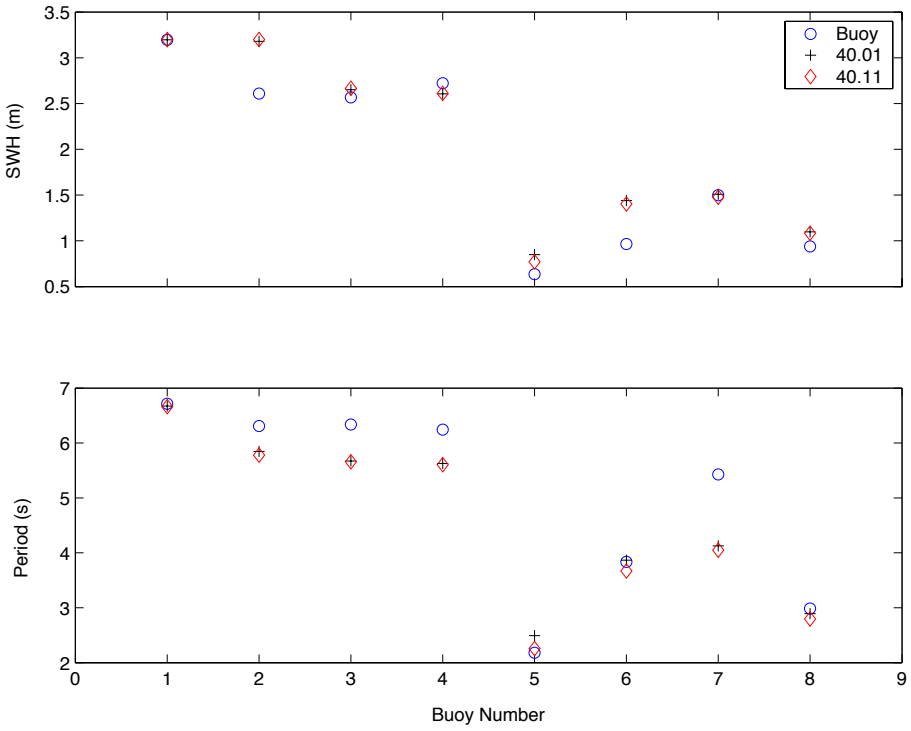

Fig. 3 — SWAN output and buoy data comparisons for significant wave height and mean wave period for Test 1, Case 2, which represents wind speed and direction at 12 m/s and 300 deg on 10/14/82 at 22.00 h UTC

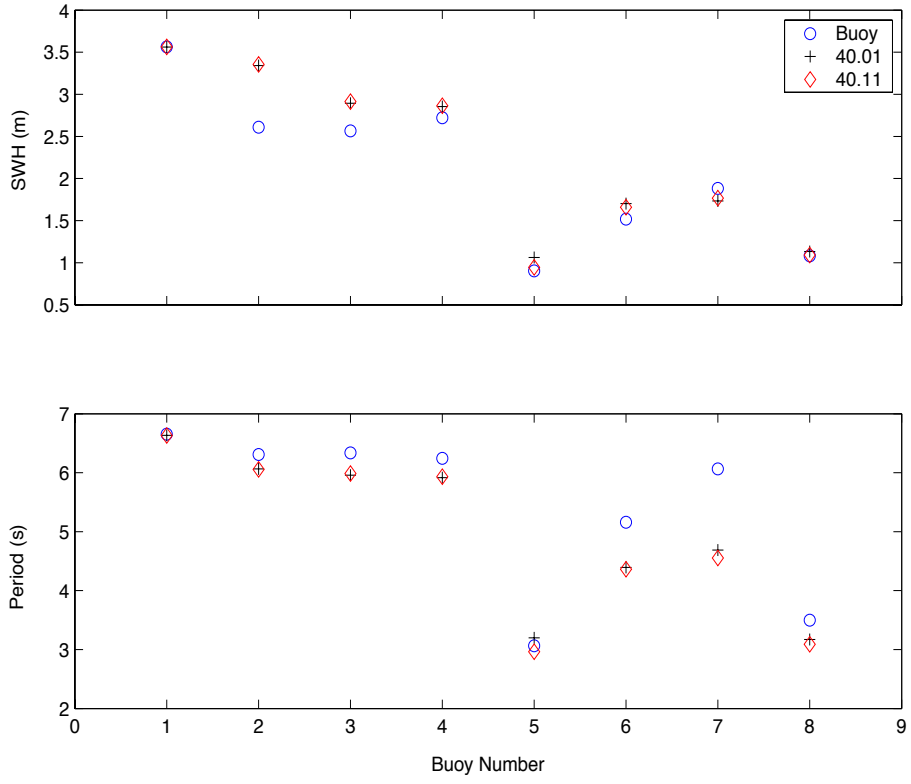

Fig. 4 — SWAN output and buoy data comparisons for significant wave height and mean wave period for Case 3, which represents wind speed and direction at 14 m/s and 300 deg on 10/14/82 at 23.00 h UTC

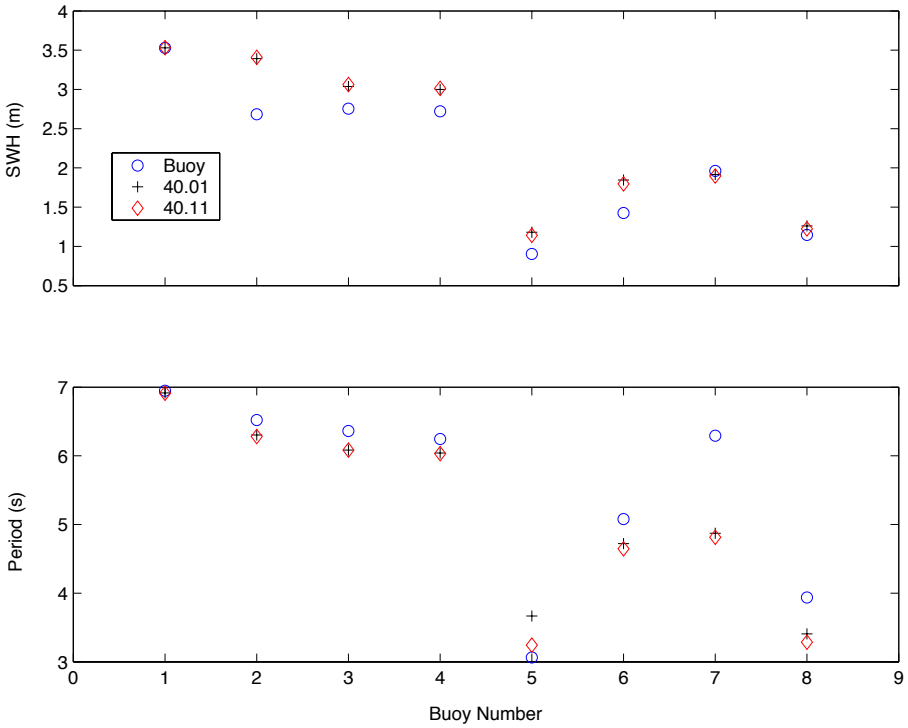

Fig. 5 — SWAN output and buoy data comparisons for significant wave height and mean wave period for Case 4, which represents wind speed and direction at 15 m/s and 300 deg on 10/14/82 at 24.00 h UTC

When compared, there was a sufficient agreement between the computed spectra and the observed spectra around 2300 UTC, particularly when allowing for the large variation in scale of the spectra (e.g., Station 5 with a twenty-fold change in energy scale compared to Station 1). Nevertheless, the decay of the primary peak and the regeneration of high-frequency energy were overpredicted. Repeated computations verified that water level variations during the residence period of the waves could not explain the discrepancies at the low frequency peak. However, it must be stressed that only small residuals of low-frequency energy were compared. The regeneration at high frequencies may have been caused by too much energy transfer from the lower frequencies by triad wave-wave interactions or by too much generation by wind. Repeated computations without triad wave-wave interactions but with wind and vice versa showed that both processes were equally responsible for this high frequency regeneration. In other cases, a similar phenomenon of overpredicting the regeneration of high-frequency energy occurred. The errors at the low- and high-frequency side of the spectrum compensated roughly to produce a correct significant wave height, but in fact were the main cause for underpredicting the mean wave period.

3.2 Test 2: Friesche Zeegat, the Netherlands

3.2.1 Purpose

Test 2 was performed to verify the wave model (Version 40.01) in a complex bathymetry in the field with tidal currents. A complete description of the test area, model setup, and comparison results can be found in Booij et al. (1999) and Ris et al. (1999).

3.2.2 Test Characteristics

Test 2 consisted of data analysis of data collected in the Friesche Zeegat on October 9, 1992. The Friesche Zeegat is located approximately 70 km west of the Norderneyer Seegat, between the islands of Ameland and Schiermonnikoog in the northern part of the Netherlands. The bathymetry, 15 km × 25 km, is rather complex, with a water depth varying from about 2 m over the shoals at high tide to about 15 m in the tidal channels (see Fig. 6).

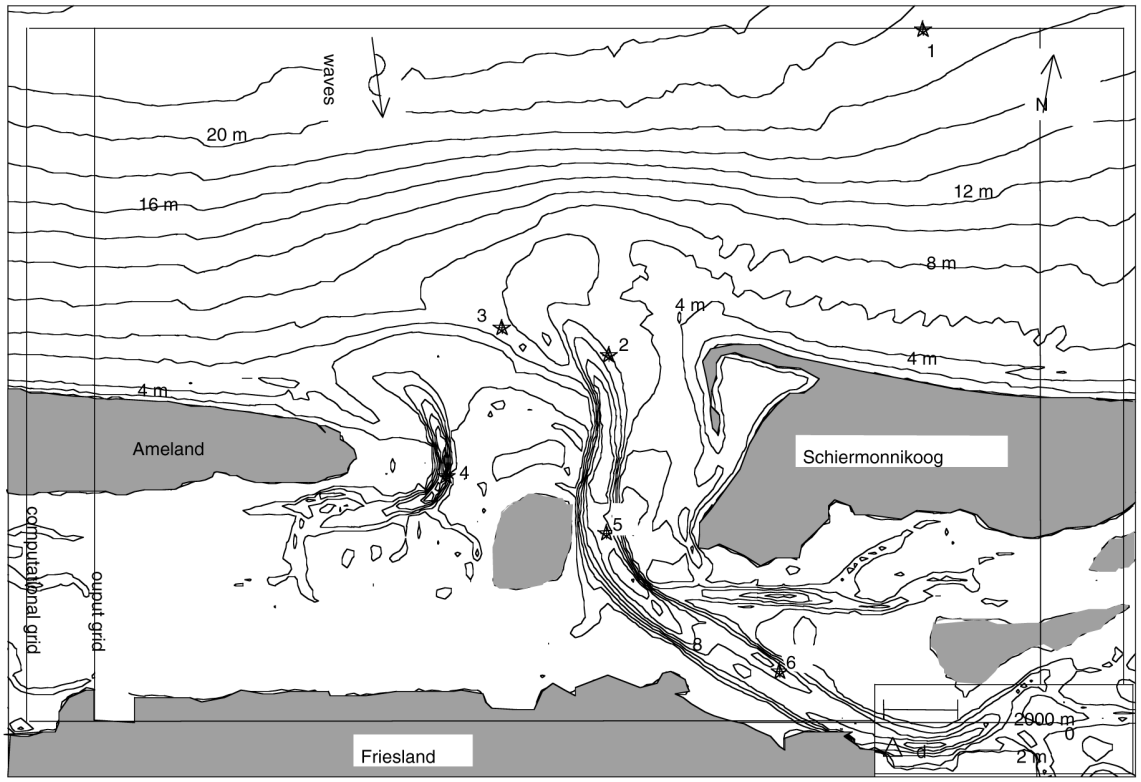

Fig. 6 — Bathymetry and data locations for Test 2

Test 2 compares the computed and observed data of the Friesche Zeegat flood case. The data were collected by the Ministry of Transport, Public Works and Water Management. The Friesche Zeegat was selected because observations were available in conditions with tidal currents computed with a fair amount of detail. For this test, the following observations were selected from the data set:

- Case (a) at 0500 UTC represented the flood current with $U_{10} = 11.5$ and direction of 310 deg;
- Case (b) at 0900 UTC represented the high water case with $U_{10} = 10$ and direction of 280 deg;
- and Case (c) at 1100 UTC represented the ebb current case with $U_{10} = 11.5$ and direction of 290 deg.

These cases were chosen, because 1) at these times, relatively high waves were observed (significant wave height in deep water of 3 m); 2) during the period of the observations the wind speed was nearly constant; 3) the incident frequency spectrum was unimodal; 4) tidal currents and water levels were measured; and 5) the observations at the different stations were carried out simultaneously (avoiding synchronization problems). As the waves penetrated through the tidal gap, they refracted out of the channels, across the shoals of the tidal flat. Behind the barrier islands, the waves completely reversed their direction due to refraction, where they were regenerated by the local wind. It appears that the offshore waves (for the case

considered here) hardly penetrated into the interior region because of the strong filtering effect of the shallow banks in the middle of the tidal gap. The wind velocity and direction were recorded at a station located north of Schiermonnikoog. The wind speed and direction, assumed to be uniform over the area, and the incident wave conditions are given in Table 6. The size, range, and resolution of the computational grid are given in Table 7. The current velocities and water levels that were used in the computations were obtained with the Water Quality/Circulation Model (WAQUA) (Les 1996; Stelling et al. 1986). In the SWAN computation, all physical processes except wave-induced setup were taken into account.

Table 6 — Wind and Incident Wave Conditions

Test Area	$H_{s,i}$ (m)	$T_{m01,i}$ (s)	$\theta_{wave,i}$ (deg)	$\sigma_{\theta,i}$ (deg)	U_{10} m/s^{-1}	θ_{wind} (deg)
Friesche Zeegat						
Flood	2.24	5.6	328	31	11.5	320
Ebb	3.31	7.4	341	23	11.5	340

The variables are defined as $H_{s,i}$, incident significant wave height; $T_{m01,i}$, mean wave period; $\theta_{wave,i}$, mean wave direction; $\sigma_{\theta,i}$, directional spreading; U_{10}, wind speed; and θ_{wind}, wind direction for the verification cases of this study. Wind and wave directions represent directions winds and waves are coming *from*.

Table 7 — Size, Range, and Resolution of the Computational Grids

Geographic Grid	
Size (km)	31.0 × 18.8
Resolution (m)	250 × 250
*Spectral Grid**	
Range in f (Hz)	0.052 to 1
Range in θ (deg)	0 to 360
Resolution	$\Delta f = 0.1f$, $\Delta\theta$ = 10 deg

Here f is spectra wave frequency; θ is spectral wave direction

* Above the maximum frequency, an f^{-4} tail is added to the spectrum

3.2.3 Results

The values in Tables 8 and 9 show that SWAN performed well in Test 2 for significant wave height and mean wave period, respectively. Comparisons between the wave buoys, SWAN 40.01, and SWAN 40.11 model results are given in Figs.7 through 9 for Test 2, Cases 1 through 3, respectively.

The computed pattern of the significant wave height and the mean wave direction for the flood case (0500 UTC) was consistent with the pattern from the observed data. Between the deepwater boundary and the entrance of the tidal inlet, the wave height gradually decreased. Results of repeated computations (with and without wind) showed that wind generated more wave energy in the deeper, eastern entrance than in the shallow, western entrance of the tidal inlet (suggesting that the waves penetrated deeper into the eastern channel than the western). After the waves traveled through the tidal gap between the two barrier islands, they refracted laterally to more shallow parts of the inlet, while completely reversing their direction behind the two islands. The similarity between the observed significant wave heights was sufficient, but the mean wave period was underestimated by approximately 1 s. The computed mean wave directions at Stations 2 and 3 differed by 1 and 3 deg, respectively, from the observed directions.

Table 8 — SWAN Test 2 Performance for the Significant Wave Height H_s

	$H_{s,i}$ (m)	H_s (m)	*Bias* (m)	*RMS* (m)	*SI*
Friesche Zeegat					
Flood	2.24	1.01	0.09	0.14	0.14
Ebb	3.31	1.12	0.14	0.47	0.42

Abbreviations are defined as $H_{s,i}$, incident significant wave height; H_s, mean observed significant wave height; and *SI*, scatter index.

Table 9 — SWAN Test 2 Performance for the Mean Wave Period T_{m01}

	$T_{m01,i}$ (s)	T_{m01} (s)	*Bias* (s)	*RMS* (s)	*SI*
Friesche Zeegat					
Flood	5.6	3.9	-0.8	0.8	0.22
Ebb	7.4	5.0	-0.6	0.7	0.15

The incident mean wave period is $T_{m01,i}$, the mean observed wave period is T_{m01}, and *SI* is the scatter index

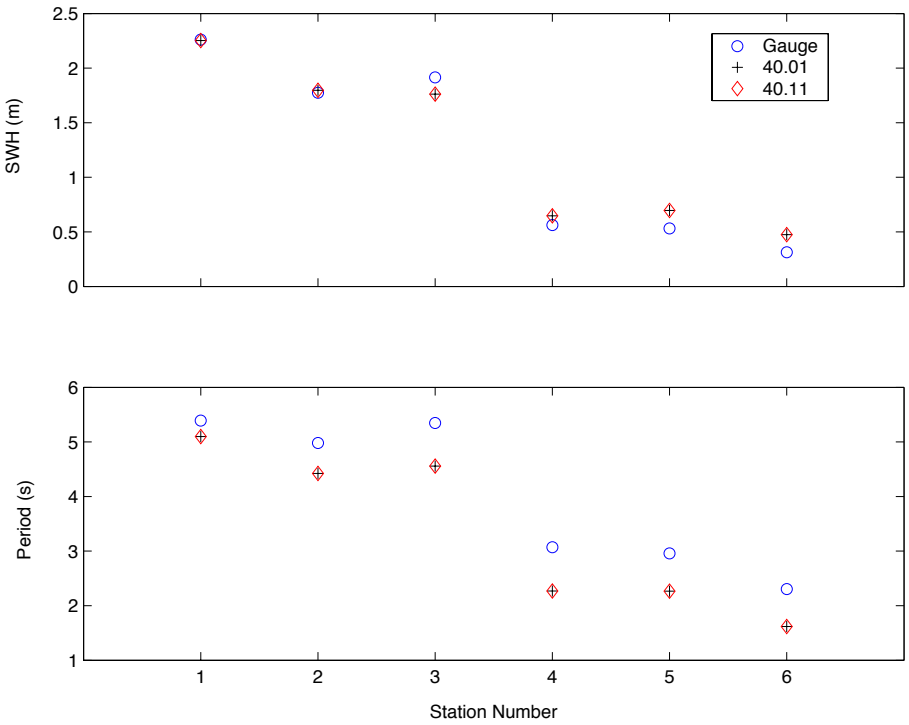

Fig. 7 — Results of comparison between SWAN model output and observations for significant wave height and mean wave period for Case 1, which represents the flood current with U_{10} = 11.5 and direction of 310 deg

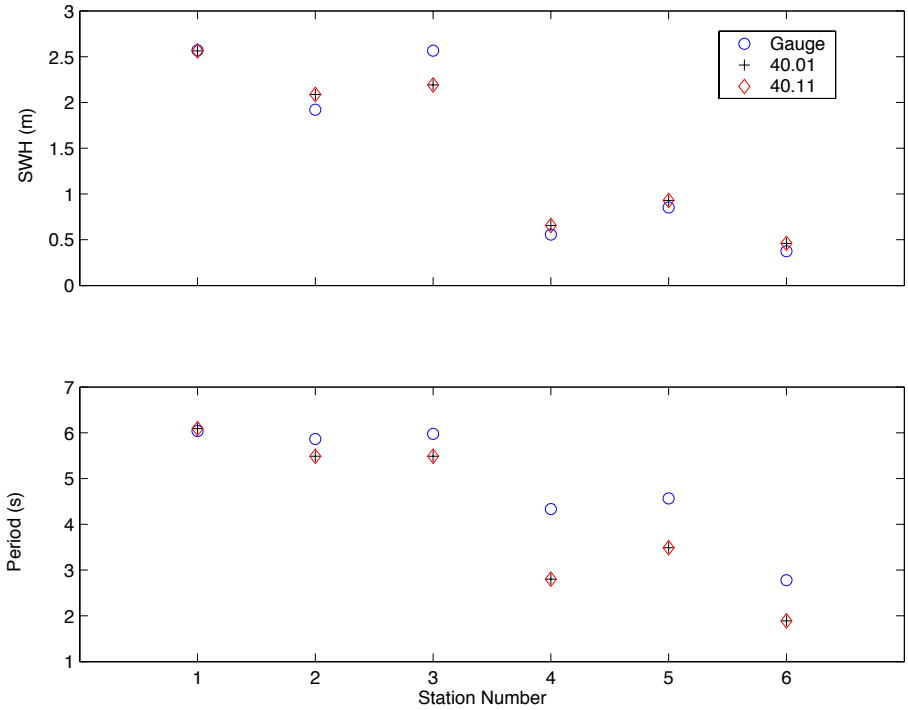

Fig. 8 — Results of comparison between SWAN model output and observations for significant wave height and mean wave period for Case 2, at 0900 UTC, which represents the high water case with U_{10} = 10 and direction of 280 deg

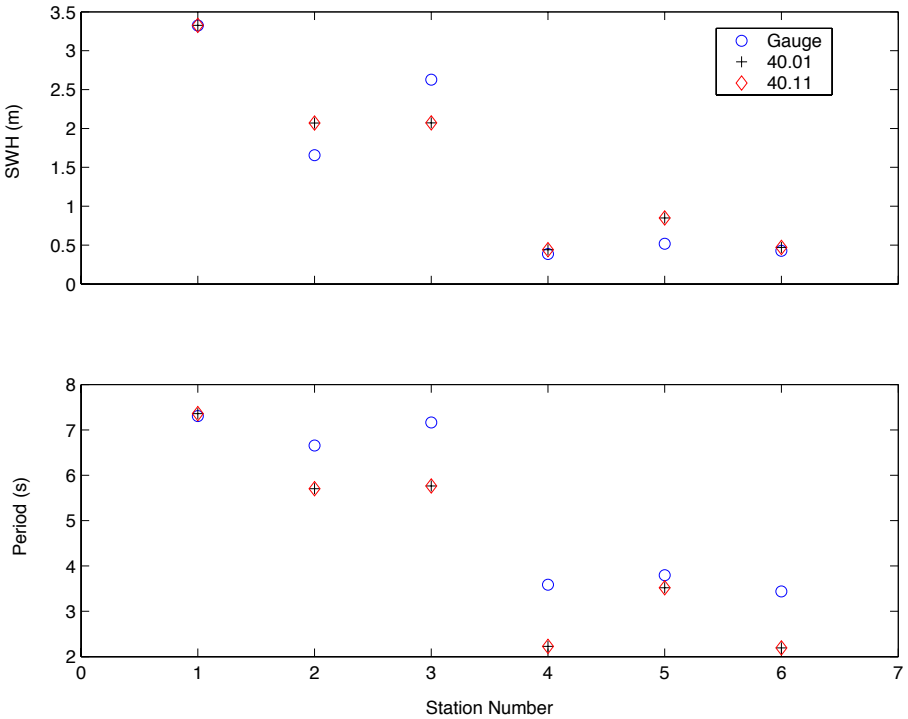

Fig. 9 — Results of comparison between SWAN model output and observations for significant wave height and mean wave period for Case 3, at 1100 UTC, which represents the ebb current case with U_{10} = 11.5 and direction of 290 deg

Computations showed that the effect of the currents in the area was a decrease in the significant wave height and mean wave period in the channels. For instance, at Station 5 the currents reduced the significant wave height from 0.8 to 0.6 m and the mean wave period from 2.9 to 1.9 s. The presence of currents in the model reduced the agreement with the observed mean wave period. Currents slightly affected the mean wave direction with differences of 10 deg at Stations 4 and 5. Computations showed that in the model the wind was important in the inner region where waves at Station 6 were regenerated (significant wave height 0.13 m without wind and 0.52 m with wind), but this regeneration was overestimated, resulting in high significant wave heights and low mean wave periods. Repeated computations with various source terms activated and deactivated showed that the gradual decrease of the significant wave height north of the barrier islands and over the tidal flats was due to depth-induced wave breaking. The agreement between the observed and computed spectra was better in this case than in the Norderneyer Seegat cases. The decay of the low-frequency peak was overpredicted (at Stations 2 and 3), but the total energy involved in the relevant frequency band (0.13 to 0.16 Hz) was relatively small. In view of the water depth, triad wave-wave interactions seemed to be relevant only at Stations 2 and 3, where the high-frequency level of the computed spectra agreed well with the observed high-frequency level. The overprediction of the regeneration of high-frequency energy was not as obvious as in Test 1 (except at Station 6).

The computed pattern of the significant wave height of the ebb case was similar to that of the flood case, except that shoals in the tidal gap blocked wave penetration into the area (the water level was 1.25 m lower than in the flood case) and the currents acted as a wave guide (resulting in somewhat higher waves over the channels and mean wave directions that roughly followed the channels). When the computed significant wave height and mean wave period were compared to the observed values, it was evident that the agreement between the observed and computed significant wave height was variable, whereas the computed wave periods were generally too low. The computed mean wave direction at Stations 2 and 3 differed by 2 deg and 1 deg, respectively, from the observed directions (this matter was trivial considering these stations are located seaward from the shallow area). The agreement between the observed and computed spectra in the ebb case was slightly better than in the flood case.

3.3 Test 3: Lake George, Australia

3.3.1 Purpose

The purpose of Test 3 was to study the performance of SWAN in the idealized depth-limited wave growth situation of Lake George, near Canberra, Australia. A more thorough discussion of Test 3 characteristics and results is given in Padilla-Hernandez and Monbaliu (2001).

3.3.2 Test Characteristics

Test 3 was taken from the data analysis of Lake George, Australia from April 1992 through October 1993. Lake George is shallow with a relatively uniform bathymetry (approximately 2 m depth; see Fig. 10). It is approximately 20 km long and 10 km wide. The bottom is smooth and composed of fine clay (Ris 1997). The water level varies with the season.

To test the performance, the 2-D mode was used. Three northerly wind cases were selected to compare with the computed data. These three cases are typical examples: a relatively low wind speed (U_{10} = 6.5 m/s), a medium wind speed (U_{10} = 10.8 m/s), and a high wind speed (U_{10} = 15.2 m/s). The computations were carried out with SWAN Version 40.01 using the WAM Cycle 3 formulations (Booij et al. 1999). The SWAN model was run with the three formulations originally included plus the eddy-viscosity formulation of Weber. The data of Lake George, collected by a series of eight wave gauges placed along the North-South axis of the lake, were used to tune the friction coefficients of every formulation such that the combined scatter index

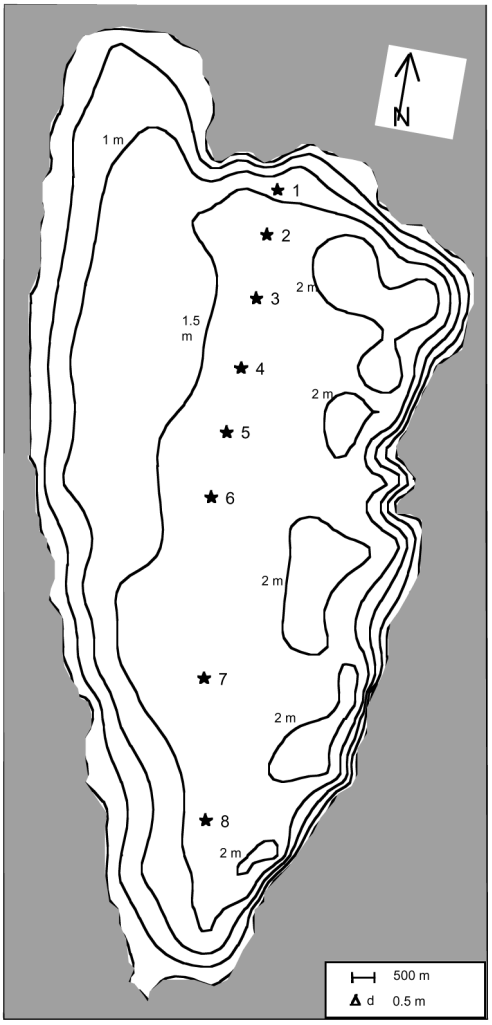

Fig. 10 — Bathymetry and data locations for Test 3

was minimal. Only the data for which the wind speed and direction were relatively constant during the 30-min sampling period have been retained. The criteria for this test were set so that the wind speed should not vary more than 10 percent nor should the wind direction change more than 10 deg to each side of the alignment of the instrument array during the 30-min sampling period.

The wave-wave triad interactions and depth-induced wave breaking were turned on with default parameter values. Station 1 was taken as the up-wave boundary in the simulation (avoiding uncertainty in the location of the northern shore because of seasonal variation in water depth). Since no directional wave spectrum was available at Station 1, the directional distribution of the waves was approximated with $\cos^2(\theta)$. For the computations, a direction resolution of 10 deg and a logarithmic frequency resolution between 0.166 and 2.0 Hz for the low wind case and 0.125 and 1.0 Hz for the medium and high wind cases were selected. The spatial resolution was 250 m in the *x*- and *y*-directions. The water level was increased over the entire lake to +0.1, +0.3, and +0.27 m for the low, medium, and high wind cases, respectively, to account for seasonal variations. The physical processes of depth-induced wave breaking, bottom friction, triads, quadruplets, and wind were activated in SWAN.

Once the appropriate values for the friction coefficients and roughness length were chosen, the other two selected cases for Lake George were run using these values. It was assumed that the bottom condition did not change.

3.3.3 Results

Figures 11 through 13 demonstrate SWAN capabilities to model significant wave height and peak period at varying wind speeds as compared to wave gauge data from eight locations. Case 1 was for low wind speed, Case 2 was for medium wind speed, and Case 3 was for high winds. The figures show comparisons between gauge data, SWAN 40.01, and SWAN 40.11 for Test 3.

The significant wave height and peak period were relatively well modeled by SWAN using any of the four friction models, except at the last three stations in the low wind speed case. At these stations (6 to 8), the wave parameters did not show a monotonic behavior, which is attributed to unresolved variation in the wind field. A boundary layer parameterization was used in creating the wind input files; however, it did not adequately produce ideal wind fields for the southern half of the model domain. Stations 6, 7, and 8 were, therefore, eliminated from the statistical calculations for the low wind case. A minor underestimation of T_p (peak wave period) was observed in the medium and low wind cases. The results from all three SWAN runs were, to an extent, similar. The statistics showed that, using the formula of Collins (1972), SWAN gave the best approximation for H_s (significant wave height) but a poor approximation for T_p (wave period).

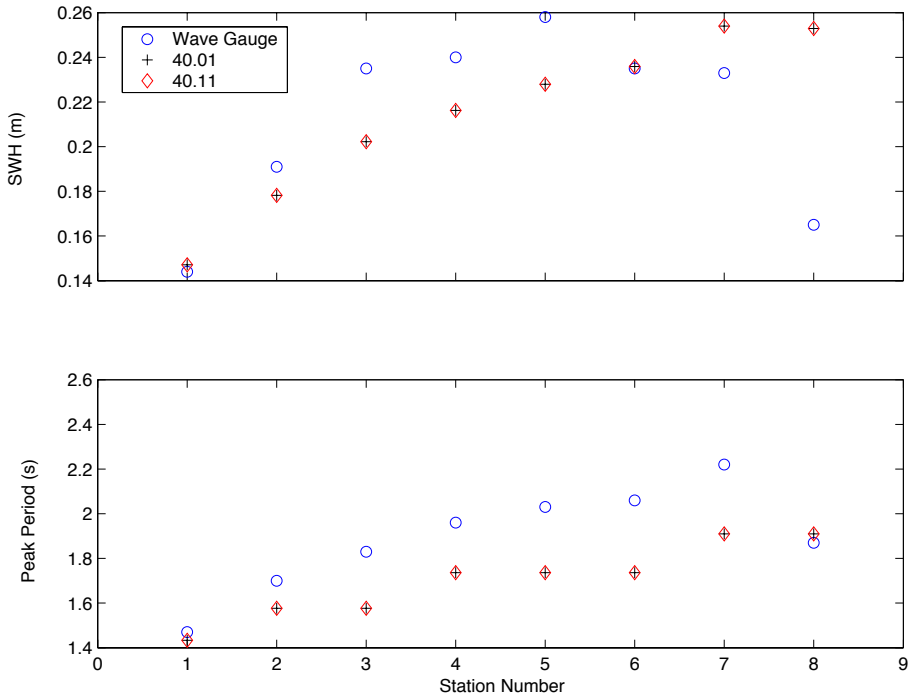

Fig. 11 — Case 1 (low wind speed (U_{10} = 6.5 m/s)) comparison of wave gauge data and SWAN output for significant wave height (SWH) and peak period

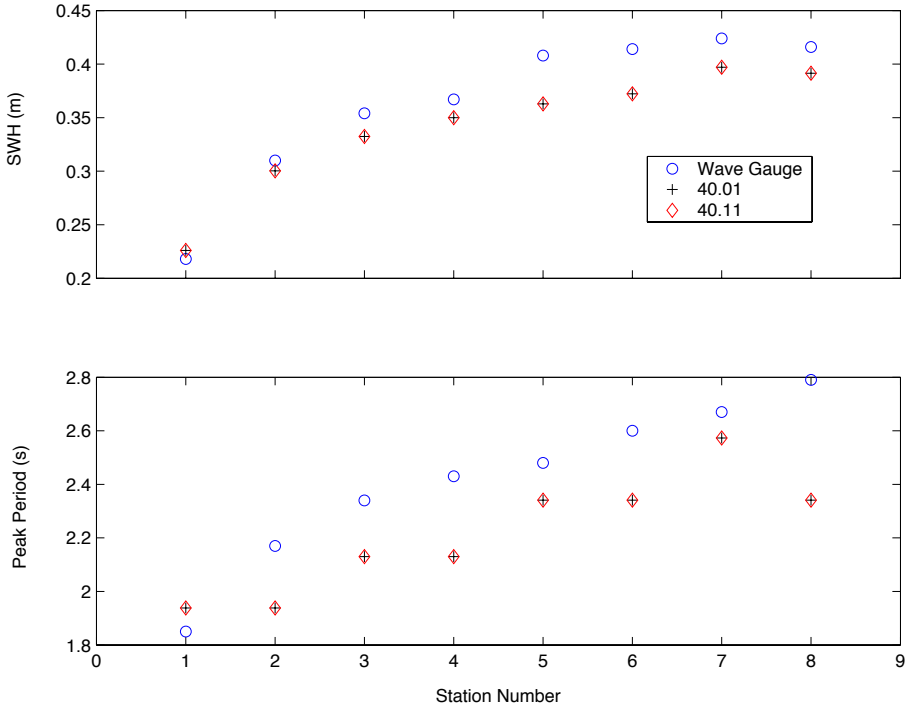

Fig. 12 — Case 2 (a medium wind speed (U_{10} = 10.8 m/s)) comparison of wave gauge data and SWAN output for significant wave height (SWH) and peak period

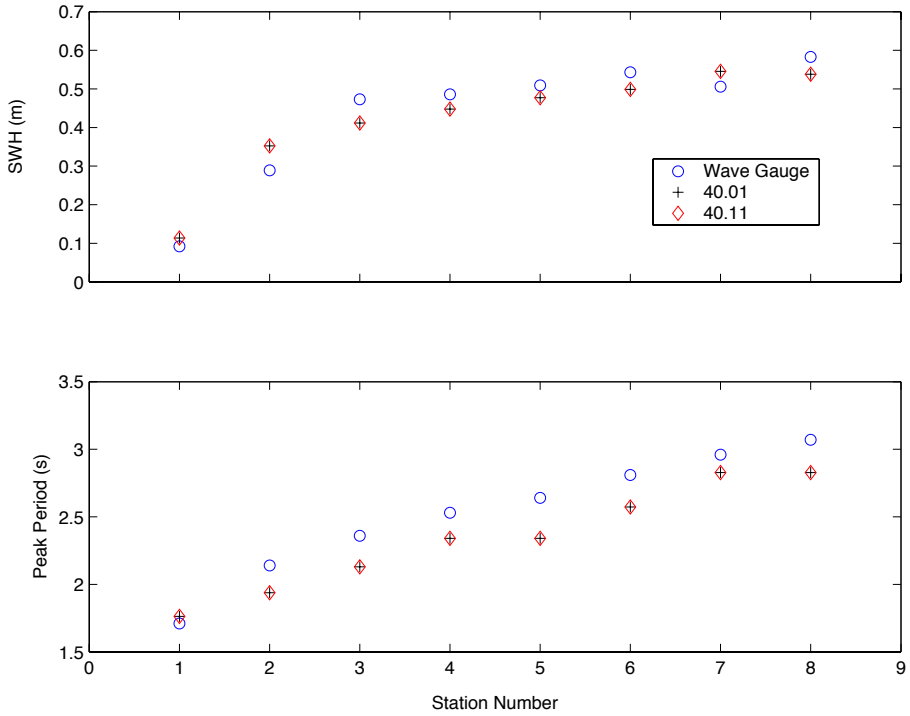

Fig. 13 — Case 3 (a high wind speed (U_{10} = 15.2 m/s)) comparison of wave gauge data and SWAN output for significant wave height (SWH) and peak period

Using the four bottom friction dissipation expressions of Collins (1972), JOint North Sea WAve Project (JONSWAP) (1973), Madsen et al. (1988), and Weber (1991), the largest error for H_s was in the high wind case when compared with the low and medium wind cases. This is partially attributed to a deviation of the measurements from the monotonic behavior in Stations 2 and 7. Looking at the values of RMSE and SI for the three cases, the best performance for H_s corresponded to the use of the Collins formulation and the best performance for T_p corresponded to the Weber formulation. SWAN performs best when using Weber's formulation followed by the Collins, JONSWAP, and Madsen formulations. Using the formulation of Weber, the peak period in the low wind case was reproduced very well. However, this was not the case using the other three formulations.

3.4 Test 4: SandyDuck

3.4.1 Purpose

The purpose of Test 4 was to study the performance of SWAN against in situ wave data on an open coastline during a period of active wind wave growth followed by a period of decay. A thorough discussion of Test 4 characteristics and results is given in Rogers et al. (2000) and Rogers et al. (2003). Some of that material is presented here.

3.4.2 Test Characteristics

The time and location of Test 4 corresponds to that of the "SandyDuck" field experiment, conducted from September 22 to October 31, 1997 at Duck, North Carolina. Wave data sources included two National Data Buoy Center (NDBC) buoys (44014 at 47 m depth contour and buoy 44004 off the continental shelf), the Field Research Facility (FRF) "linear array" of pressure gauges (8 m depth), a set of remotely sensed data (airborne scanning lidar, Hwang et al. 2000), and other instruments deployed by various researchers.

The simulations were run on two grids, a 2 km resolution grid, extending well past the shelf break, and a nested grid, including the Duck region and extending to approximately 30 m water depth, with 125 m (East-West) by 150 m (North-South) resolution. Regional bathymetry and computation grid domains are shown in Fig. 14. In the present study, comparisons were presented only at NDBC buoy 44014. Additional comparisons (to lidar and array data) are in Rogers et al. (2000).

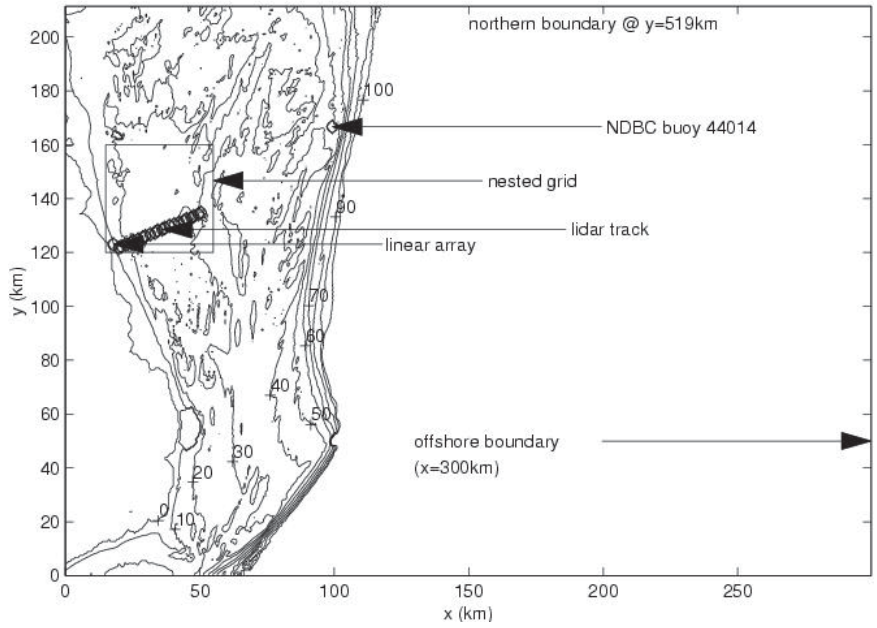

Fig. 14 — Bathymetry and data locations for Test 4

During this time period, there was a weak swell from the open ocean. Since this swell was relatively steady, the "mean swell condition" observed during the simulation period was used for boundary forcing with the larger grid. By using a stationary swell condition, it was possible to isolate (in time series plots) the effect of the model's source/sink terms on swell energy. For wind forcing, measurements came from three NDBC buoys in the region: 44014, 44004, and 44009, with linear interpolation used between the measurement locations. Winds were weak to moderate, with considerable spatial variation; during the wind event on September 24, winds were predominantly from the northeast.

3.4.3 Results

Comparisons to the lidar data by Rogers et al. (2000) indicated that while total energy was generally well predicted, mean wave period was significantly underpredicted by the model. In order to investigate this simulation error further, comparison of time series of energy at several frequencies (buoy vs model) were made. These are shown in Fig. 15. Here, model spectra were interpolated to the buoy frequencies. There were two obvious discrepancies: 1) energy at and below the spectral peak (approximately 0.18 Hz during the wind event) was underpredicted during the wind event, while energy above the spectral peak was slightly overpredicted, and 2) during the wind event, there was a sudden drop in the swell energy that was not observed in the data.

The latter discrepancy was due to the dependence of the dissipation term on the integrated wave steepness. The dissipation of the swell frequencies, previously insignificant, became significant in the presence of wind sea. The cause of the first problem was most likely a result of combined inaccuracies of the three deepwater source/sink terms and wind forcing. Rogers et al. (2003) focus on improvement via the dissipation term. However, it is not clear (from this test alone) that the dissipation term is the dominant source of error in this case. For example, wind measurements during this period of SandyDuck indicated that conditions were quite complex. Thus, there was a higher than normal level of uncertainty with regard to the wind forcing.

Figure 16 shows time series comparisons for average height (H_{m0}), average wave period (T_{mean}), and peak wave period (T_{peak}) between SWAN and NDBC buoy 44014. The notation "n=2" refers to a modification to increase dissipation of higher frequencies and decrease dissipation of lower frequencies. (This modification is suggested for general use by Rogers et al. (2003) and can be applied without modification of the source code.)

3.5 Test 5: Lake Michigan

3.5.1 Purpose

The purpose of conducting Test 5 was to explore whether the overprediction of peak wave number was a problem specific to Test 4 or if it was consistent with all SWAN model runs. A more thorough discussion of Test 5 characteristics and results is given in Rogers et al. (2003).

3.5.2 Test Characteristics

A two-part storm event that occurred during November 1995 was used to conduct the Lake Michigan test case. Observational data were available at the following four locations: 1) NDBC buoy 45002, located in the northern part of the lake in relatively deep water (greater than 100 m), 2) Coastal Marine Automated Network (CMAN) station SGNW3, located at a central latitude at the western shore, 3) NDBC buoy 45010, near the western shore, in relatively shallow water (approximately15 m), and 4) NDBC buoy 45007, the

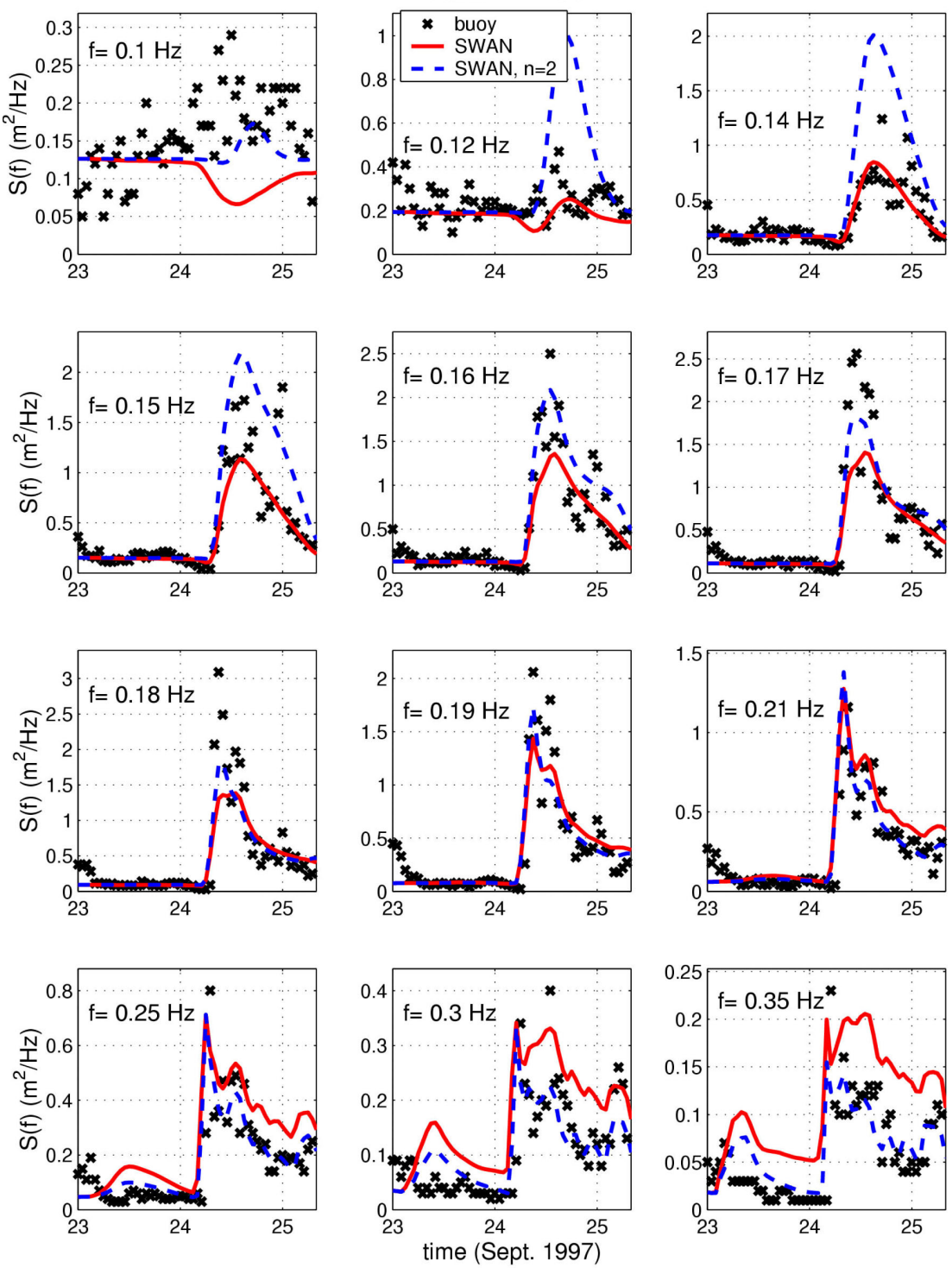

Fig. 15 — Test 4 comparison of SWAN vs NDBC buoy 44014 spectral wave energy $S(f)$ integrated over all wave directions for the frequency given in each plot. Note that scaling of ordinate axis was not constant, so the comparison was essentially normalized.

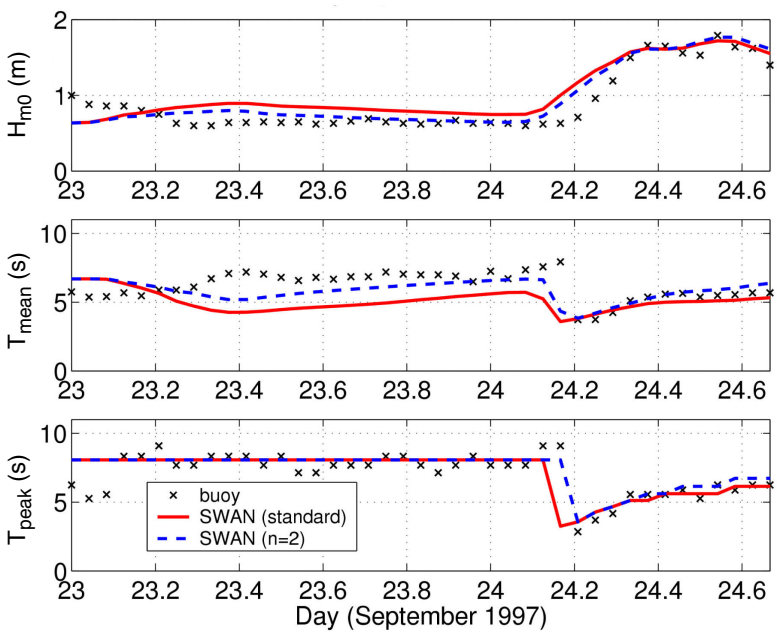

Fig. 16 — Time series comparisons for average height (H_{m0}), average wave period (T_{mean}), and peak wave period (T_{peak}) between SWAN and NDBC buoy 44014 at SandyDuck, NC.

southern deepwater buoy (depth greater than 100 m). The buoys provided wind and wave data, while the CMAN station provided only wind data. An approximately 30-hour wind event occurred, with winds generally from the South, peaking at approximately $U_{10} = 17$ m/s. After a brief lull, there was a slightly stronger event, with duration approximately 36 hours, winds predominantly from the North, and U_{10} peaking around 20 m/s. Apart from a mild sheltering effect evident in the nearshore measurements, the winds seemed to be relatively homogeneous over the lake. Air-sea temperature differences measured by the buoys were small. The lake bathymetry, which was provided by the National Oceanographic and Atmospheric Administration (NOAA) Great Lakes Environmental Research Laboratory, is shown in Fig. 17.

Both parts of the event were characterized by a growth phase (during which wind speed and wave energy grew rapidly), a brief transition phase (while wind speed was highest and source/sink, and propagation terms roughly balance), and a decay phase (when wind speed was decreasing, waves decayed via whitecapping and propagation). The decay of the second event was caused by a simultaneous decrease in wind speed and fetch length. Note that for buoy 45007, the second, northerly event was of significantly longer fetch than the first southerly event, while the opposite was true for buoy 45002. Thus, considering the buoys separately, two short fetch events and two longer fetch events were modeled with this simulation. Bulk wave parameters measured by the two buoys are summarized in Table 10.

The two events were modeled in one simulation, initialized with zero energy state at 1600 on November 8. Wind data from buoys 45002 and 45007 were used. Wind data from the two coastal data locations were not used due to the sheltering apparent in data from those locations (wave comparisons were made only at the two open-water locations, where sheltering effects are less important). Wind was assumed uniform in longitude, with variability and latitude determined by interpolation between the two data points. Model results were compared at the locations of buoys 45002 and 45007.

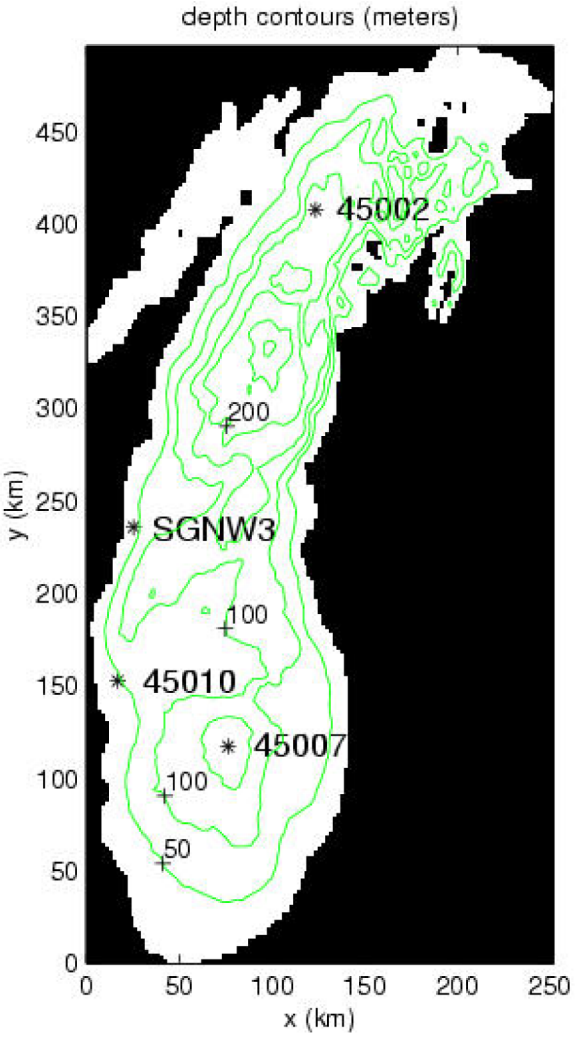

Fig. 17 — Bathymetry and data locations for Test 5

Table 10 — Bulk Parameters at the Peak of Each Event

Buoy 45007		
H_{m0} (m) 3.7, 5.2	T_p (s) 7.7, 10.0	T_{m01} (s) 7.5, 9.2
Buoy 45002		
H_{m0} (m) 4.6, 3.0	T_p (s) 10.0, 6.2	T_{m01} (s) 8.6, 6.1

Mean period, T_{m01}, was the centroid of the wave spectrum. Wave height and mean period are based on spectrum from 0.07 to 0.4 Hz.

3.5.3 Results

Three of the four model runs are compared to data in Figs. 18 and 19. Since the model used wind speeds measured at unsheltered (deepwater) locations and applied over the entire domain, it was expected that input wind speeds were higher than truth near the shoreline, where the nearby topography tended to reduce wind speeds. This discrepancy would tend to create an overprediction of wave growth. However, the error of the original model was (for the most part) an underprediction of energy in the 0.08 to 0.15 Hz range. This underprediction points clearly to a deficiency in the source/sink terms (as opposed to forcing). Wind forcing is ruled out as an error source since the winds are fairly homogeneous. A potential source of error associated with inhomogeneity would be near the shoreline where winds tend to be reduced due to topography. However, since deepwater wave buoys were used to specify winds on the model grid, overprediction of winds can not lead to underprediction of wave energy. The underprediction of low-frequency energy was most evident in the long fetch events. This was consistent with the SandyDuck simulation (see Section 3.4) suggesting that where the fetch was large (greater than100 km and wave growth was more duration-limited than fetch-limited), the model underpredicted low-frequency energy. Figures 18 and 19 show that high-frequency energy was generally well predicted, with a slight overprediction at the highest frequencies. For the short-fetch events, wave height and mean period (not shown) were generally well predicted. However, these events would be more affected by the neglect of sheltering (by nearby topography) in the wind forcing. Thus it was possible that for the short-fetch events, weak wave growth in the model was being compensated by exaggerated wind speeds near the coastline. Figures 20 and 21 show time series comparisons for average height (H_{m0}), average wave period (T_{mean}), and peak wave period (T_{peak}) between SWAN and NDBC buoys 45002 and 45007.

3.6 Test 6: Mississippi Bight

3.6.1 Purpose

The purpose of conducting Test 6 was to run SWAN in a scenario that would be similar to the manner that NAVOCEANO would be implementing the model.

3.6.2 Test Characteristics

The SWAN computational grid for Test 6 extends from 90.0 deg to 87.5 deg W and 29.0 to 30.8 deg N with a horizontal resolution of 0.025 deg. Directional wave spectra from a nested WAve Model (WAM) wave model were applied at 12 locations on the SWAN southern and eastern boundaries. Figure 22 shows the computational grid and the location of two NDBC buoys used for comparison. SWAN was initialized with a RESTART file from a previous 15-day simulation. Wind forcing was provided by Coupled Ocean Atmospheric Mesoscale Prediction System (COAMPS™) Central America grid with a 0.2 deg resolution. SWAN was run for a 30-day period, from November 1 to 30, 2002, with a 15-minute timestep, in a nonstationary mode. The bathymetry file was derived from a three-arc-second bathymetry obtained through the Navy Gulf of Mexico Littoral Initiative (NGLI) program. Tabular output is saved at two NDBC buoy locations (42007, 42040) for comparison.

3.6.3 Results

Figures 23 through 25 compare the model results to data from buoy 42040. Figures 26 through 28 show the comparisons of SWAN with buoy 42007. Tables 11 and 12 show statistics for the buoy-to-model comparisons for 42040 and 42007, respectively.

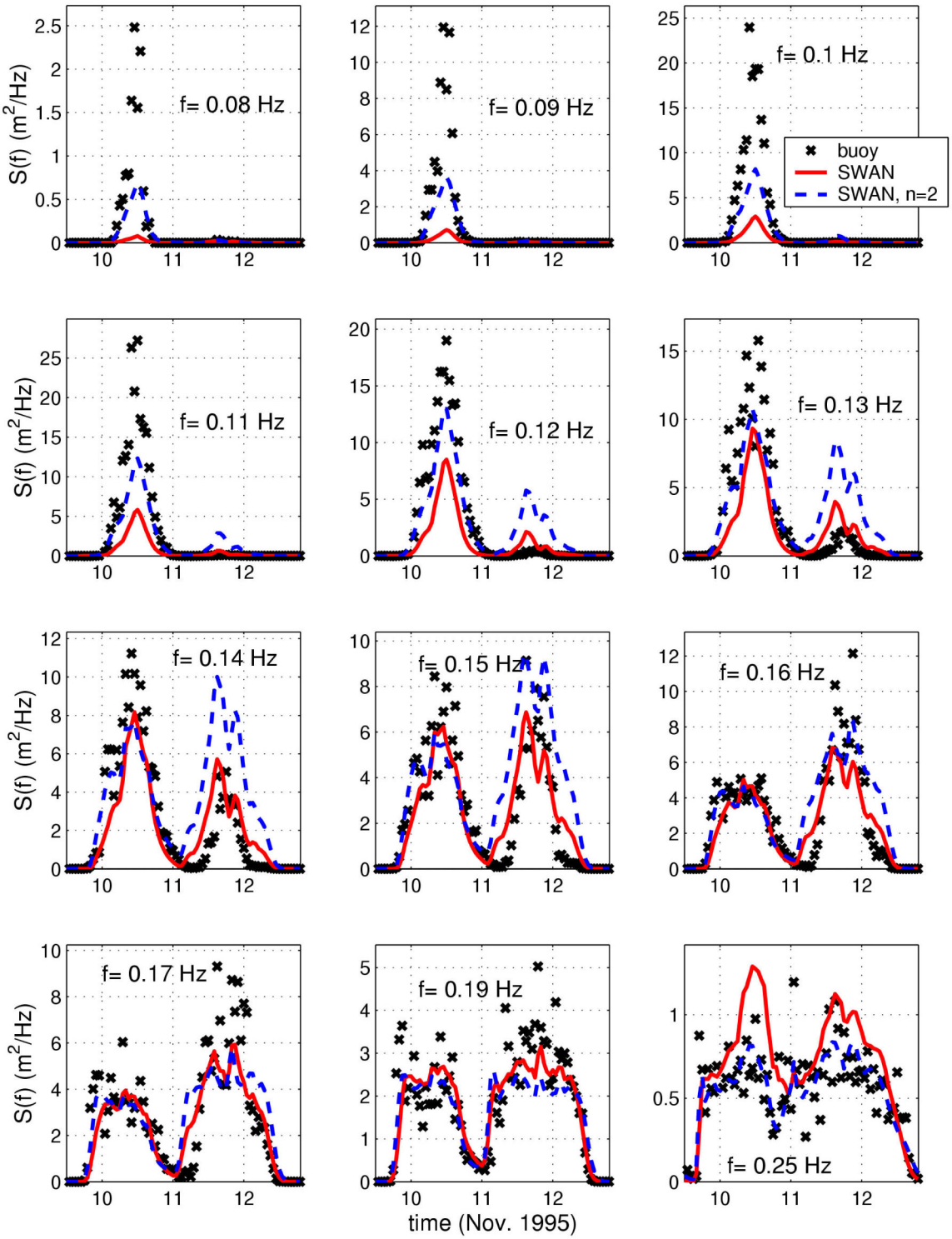

Fig. 18 — Comparison of SWAN vs NDBC buoy 45002 spectral wave energy *S(f)* integrated over all wave directions for the frequency given in each plot

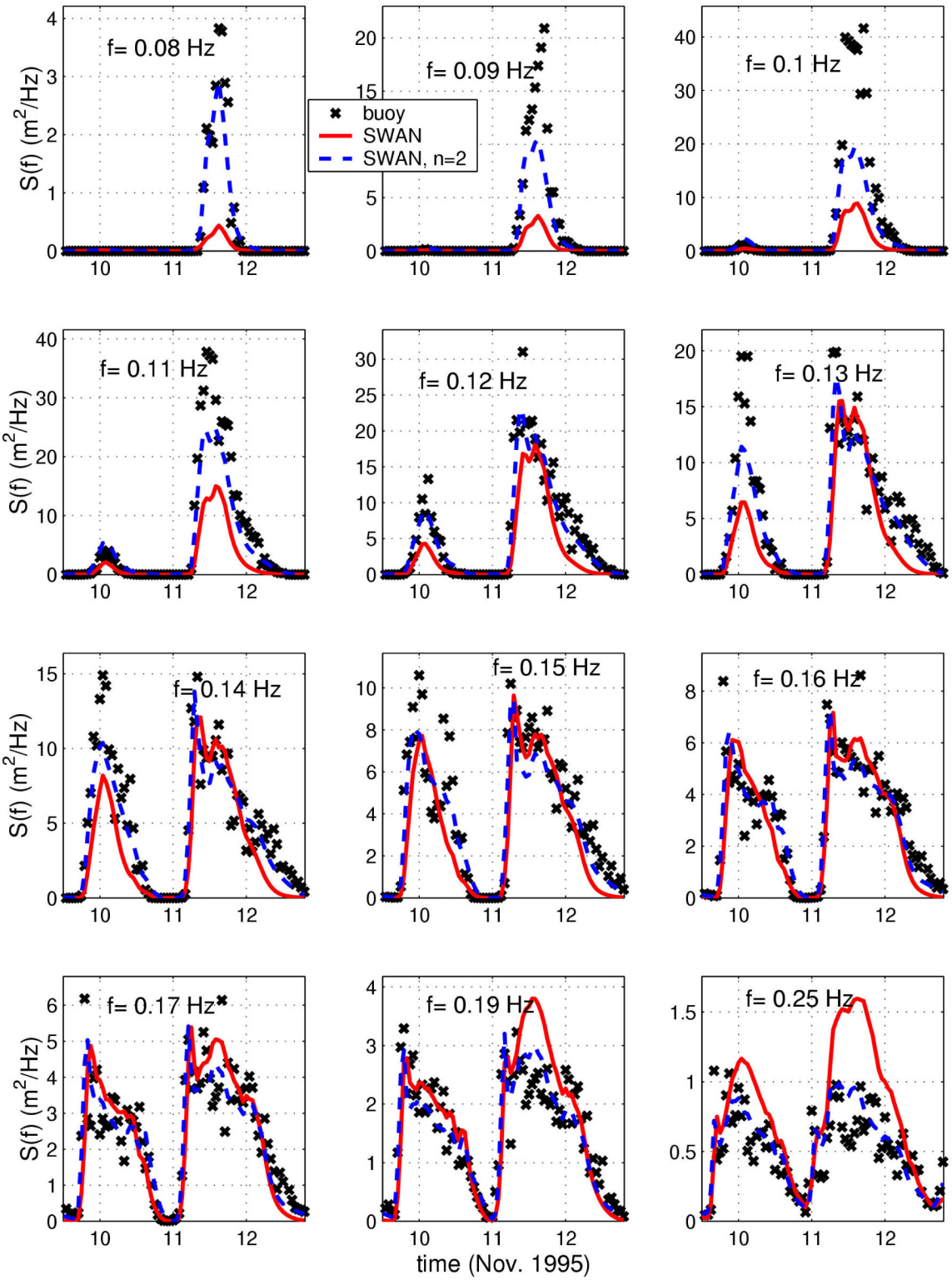

Fig. 19 — Test 5 comparison of SWAN vs NDBC buoy 45007 spectral wave energy *S(f)* integrated over all wave directions for the frequency given in each plot

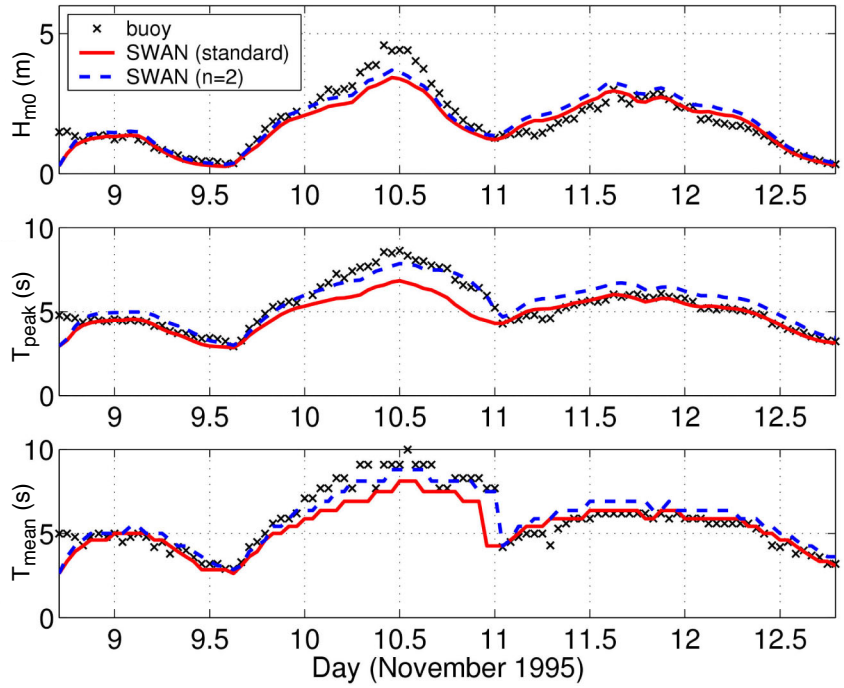

Fig. 20 — Time series comparisons for average height (H_{m0}), average wave period (T_{mean}), and peak wave period (T_{peak}) between SWAN and NDBC buoy 45002

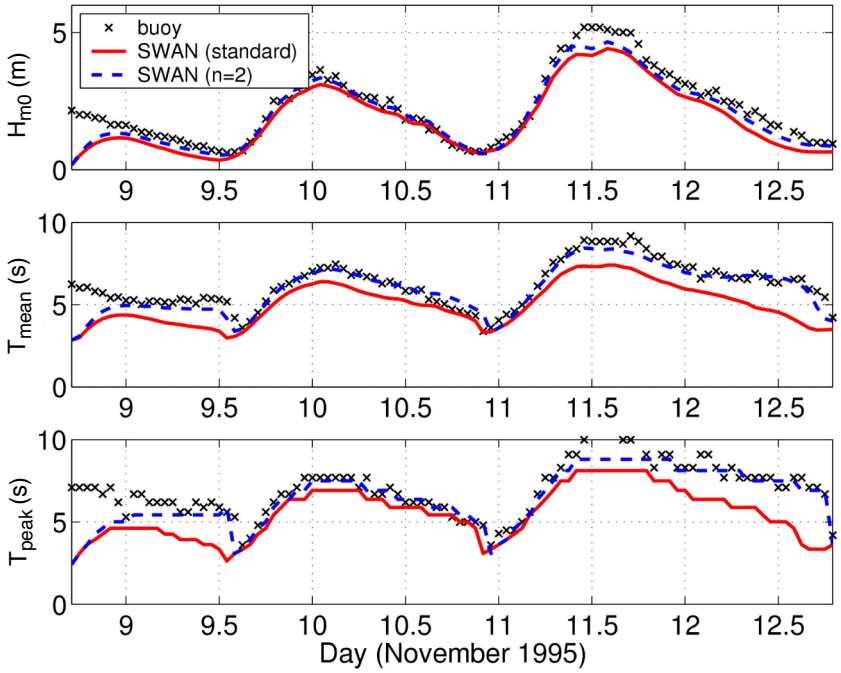

Fig. 21 — Time series comparisons for average height (H_{m0}), average wave period (T_{mean}), and peak wave period (T_{peak}) between SWAN and NDBC buoy 45007

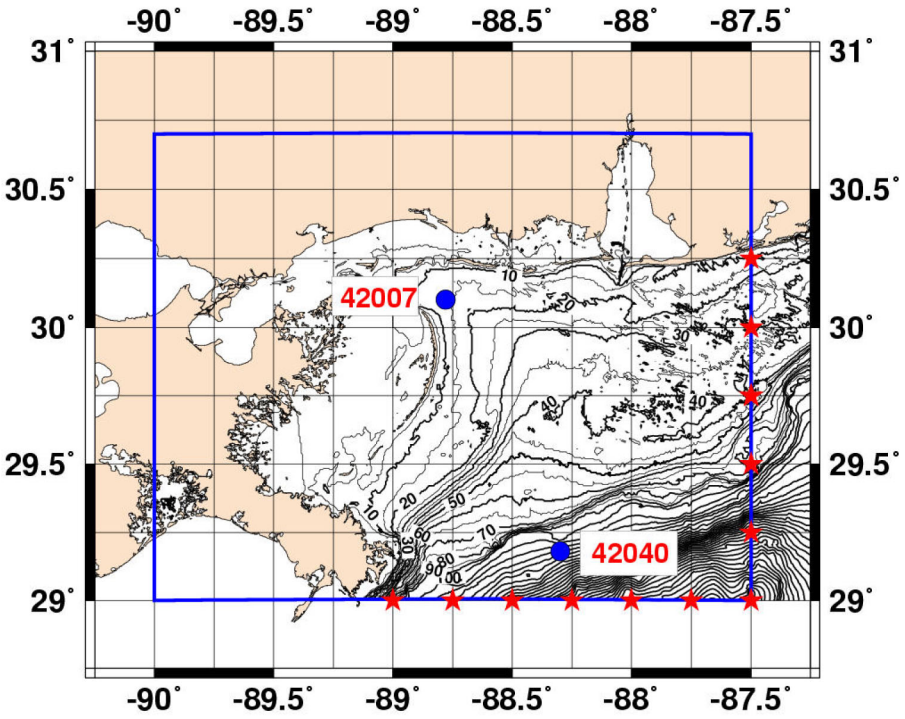

Fig. 22 — Bathymetry and station locations for Test 6. Red stars denote locations of WAM directional spectra applied on the southern and eastern SWAN boundaries. Blue circles denote NDBC buoy platforms used for model comparison.

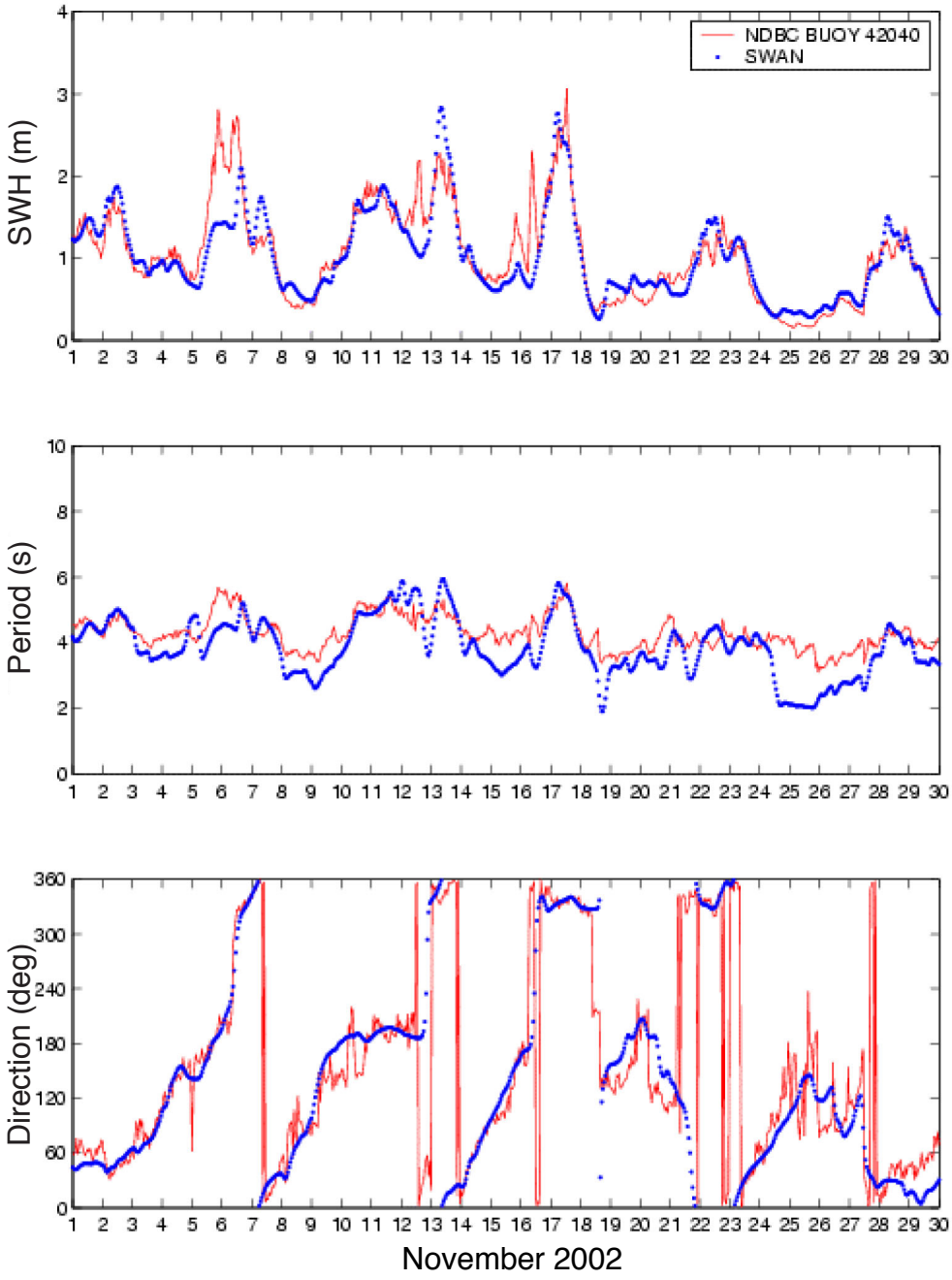

Fig. 23 — Time series comparisons for (top) average significant wave height (SWH), (middle) average wave period, and (bottom) wave direction (deg) between SWAN and NDBC buoy 42040 in the Mississippi Bight

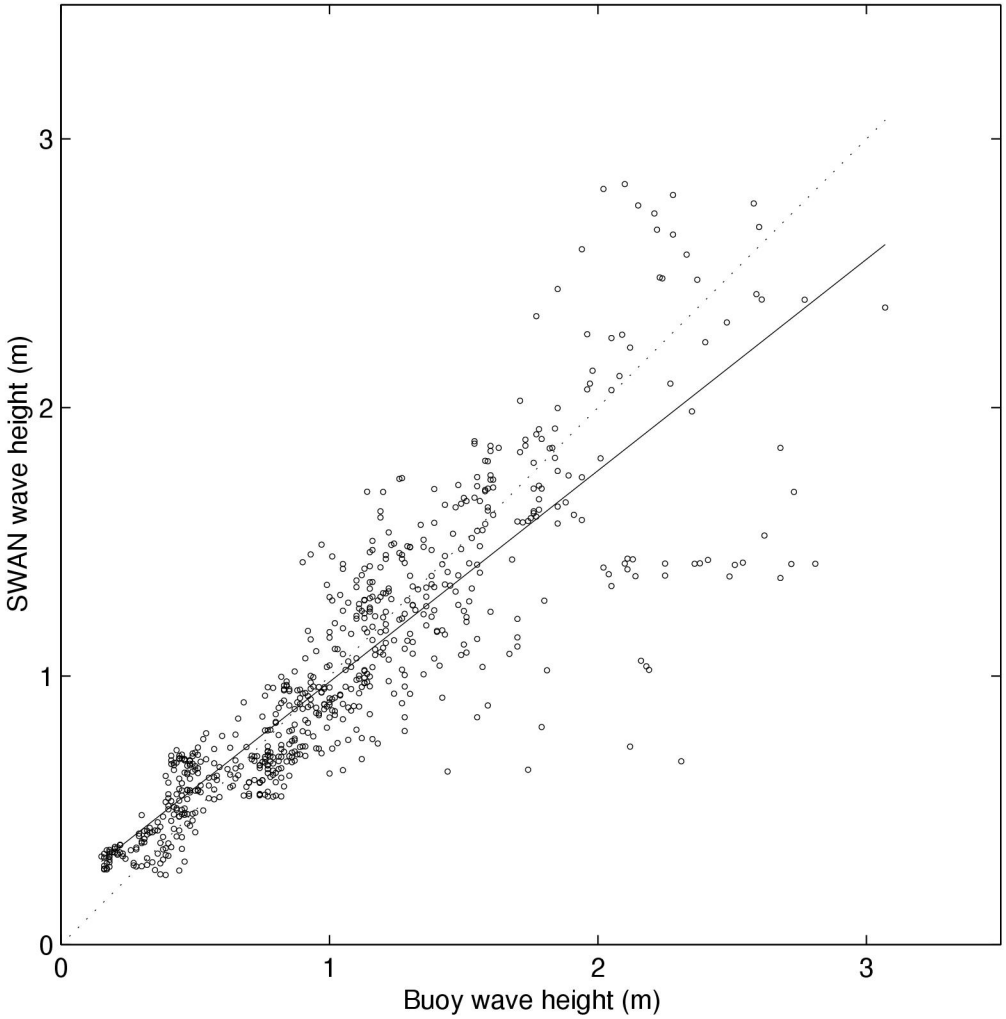

Fig. 24 — Scatterplot demonstrating the positive correlation for wave height (m) between SWAN and NDBC buoy 42040

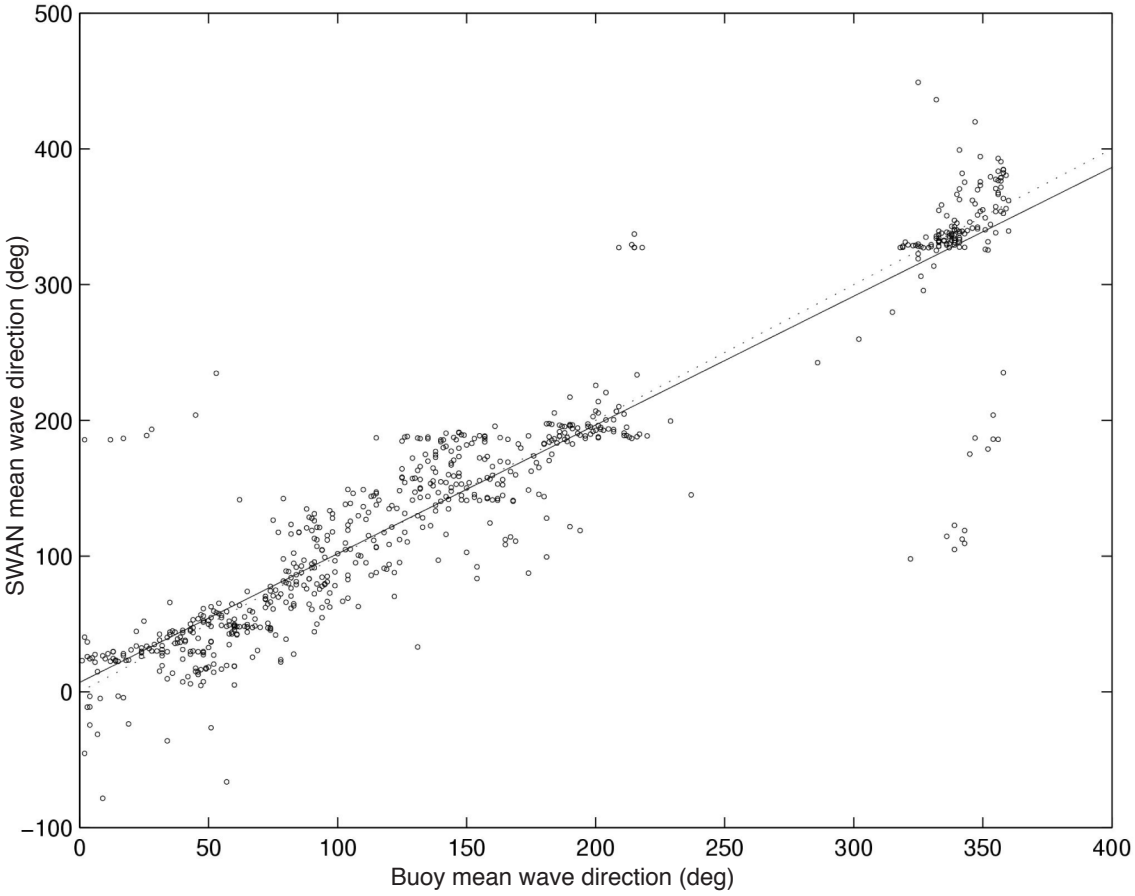

Fig. 25 — Scatterplot demonstrating the positive correlation for mean wave direction (deg) between SWAN and NDBC buoy 42040

Table 11 — Statistical Comparison between SWAN and Buoy 42040

Parameter	No. of Points	Corr. Coef.	RMS	Slope	Intercept
H_{m0}	697	.87	.29	.786	.192
T_{peak}	697	.78	.72	1.339	-1.874
Wave Direction	697	.92	42.60	.948	7.023

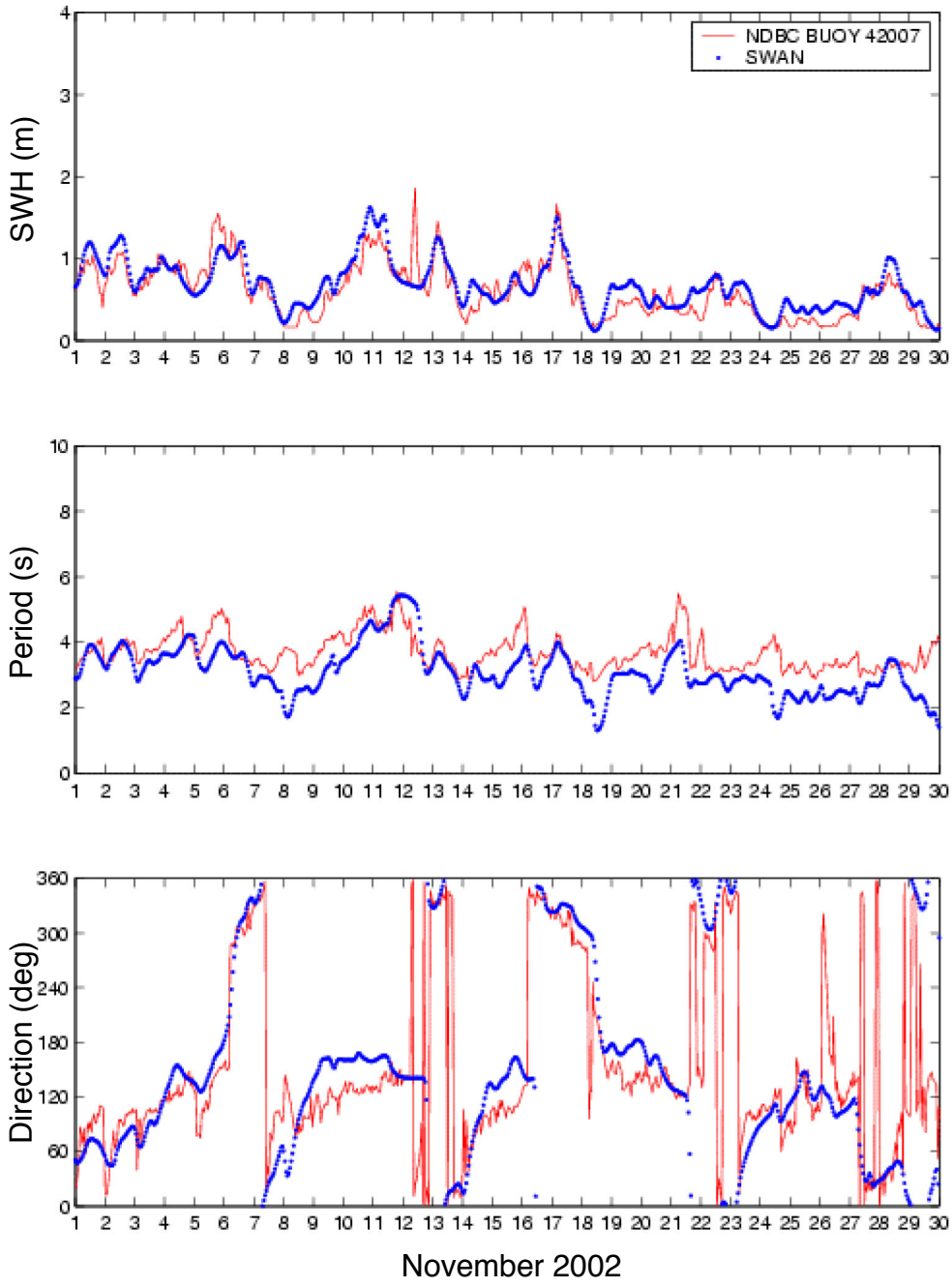

Fig. 26 — Time series comparisons for (top) average significant wave height (SWH), (middle) average wave period, and (bottom) wave direction (deg) between SWAN and NDBC buoy 42007 in the Mississippi Bight

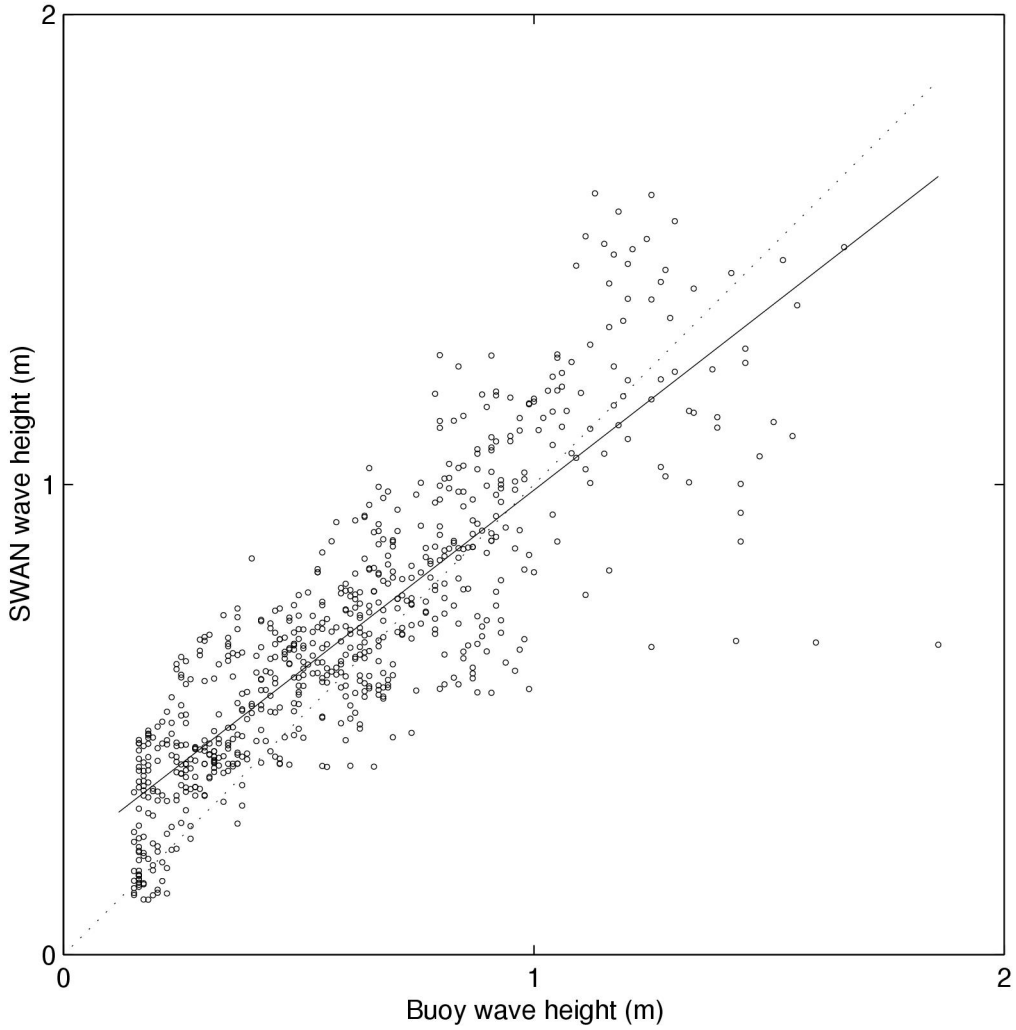

Fig. 27 — Scatterplot demonstrating the positive correlation for wave height (m) between SWAN and NDBC buoy 42007

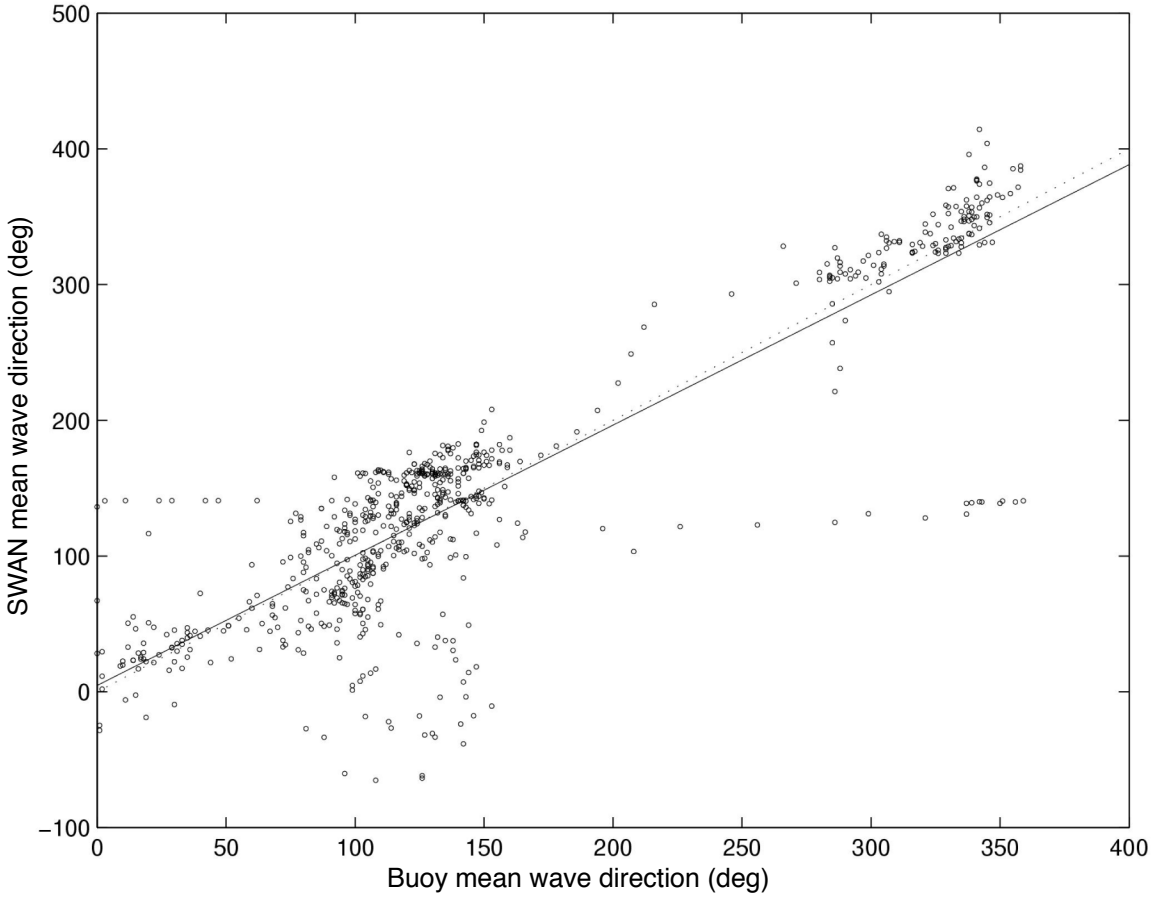

Fig. 28 — Scatterplot demonstrating the positive correlation for mean wave direction (deg) between SWAN and NDBC buoy 42007

Table 12 — Statistical Comparison between SWAN and Buoy 42007

Parameter	No. of Points	Corr. Coef.	RMS	Slope	Intercept
H_{m0}	697	.85	.19	.776	.212
T_{peak}	697	.67	.81	.930	– 0.323
Wave Direction	697	.88	50.13	.959	4.683

Overall, SWAN demonstrates a very good comparison against NDBC buoy data. The wave heights at 42040 show an RMSE of 0.29 m during the period, with a correlation of 0.87. The time series plot shown in Fig. 23 indicates an underprediction of a major storm event on November 5 and 6, 2002. Comparisons of wind magnitude at NDBC buoy 42040 shows COAMPS™ winds were underpredicted during this period. The mean wave period shown in Fig. 23 is generally within 1 s, which is the measurement error of the instrument. Statistically, the RMSE is 0.72 s with a correlation coefficient of 0.77. The mean wave direction shows favorable agreement with observations in Fig.23. The scatter plots in Figs. 24 and 25 show good agreement.

The time series plot in Fig. 26 shows excellent agreement with wave height and mean wave period for NDBC buoy 42007 located at a water depth of 13 m. Table 12 indicates an RMSE of 0.19 m and a correlation coefficient of 0.85. The mean wave period has an RMSE of 0.87 s and a correlation coefficient of 0.67. Similar to buoy 42040, the mean wave direction demonstrates a high RMSE of 50 deg, but with a high correlation of 0.87.

3.7 Test 7: Oland, Sweden

3.7.1 Purpose

Test 7 was conducted in support of North Atlantic Treaty Organization (NATO) Exercise Strong Resolve 2002.

3.7.2 Test Characteristics

SWAN was run for the Baltic Sea at a resolution of 0.1 deg during the period of March 1 through 15, 2002. A Baltic Sea Regional WAM forced with Navy Operational Global Atmospheric Prediction System (NOGAPS) provided boundary conditions at 22 locations on the western and northern boundaries of the SWAN model domain. SWAN was forced with 10 m winds from COAMPS™ Europe with a resolution of 27 km. SWAN was run with a time-step of 15 minutes. SWAN was spun-up during the period of February 25 through 28, 2002. Tides were not considered for Test 7.

SWAN wave output was saved at the location of a buoy operated by the Swedish Meteorological and Hydrographical Institute near Oland, an island off the southeast coast of Sweden. The Oland buoy was located near 56.1 deg N, 16.68 deg E in a water depth of approximately 40 m. The data record contained hourly values of significant wave height and peak wave period. Figure 29 illustrates the Test 7 area and buoy location.

3.7.3 Results

The Baltic Sea is affected by many storms, especially during the winter months. This was evident by the observation of eight peaks in wave height during the study period. On average, a storm affected this region every 2 to 3 days during the test period. SWAN showed excellent agreement with wave height throughout the period with the only exception occurring on March 8 when SWAN overpredicted by 0.4 m. SWAN also compared well with peak wave period, falling within the 1-s error associated with the buoy (see Fig. 30).

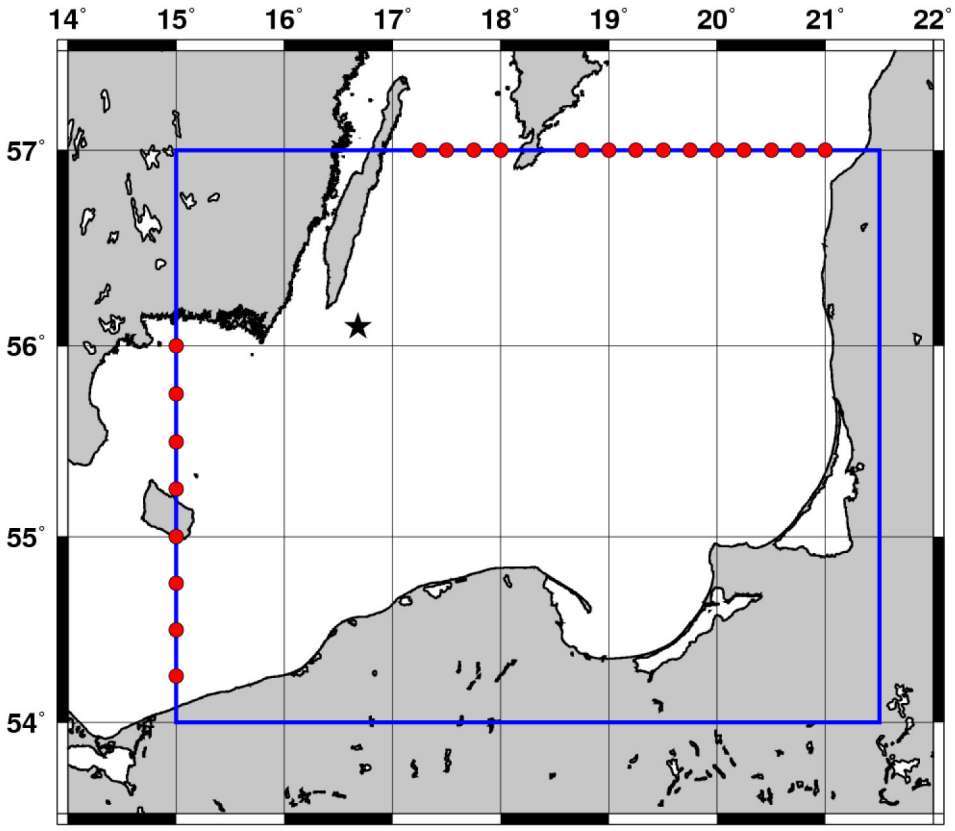

Fig. 29 — Test area and buoy location (★) for Test 7

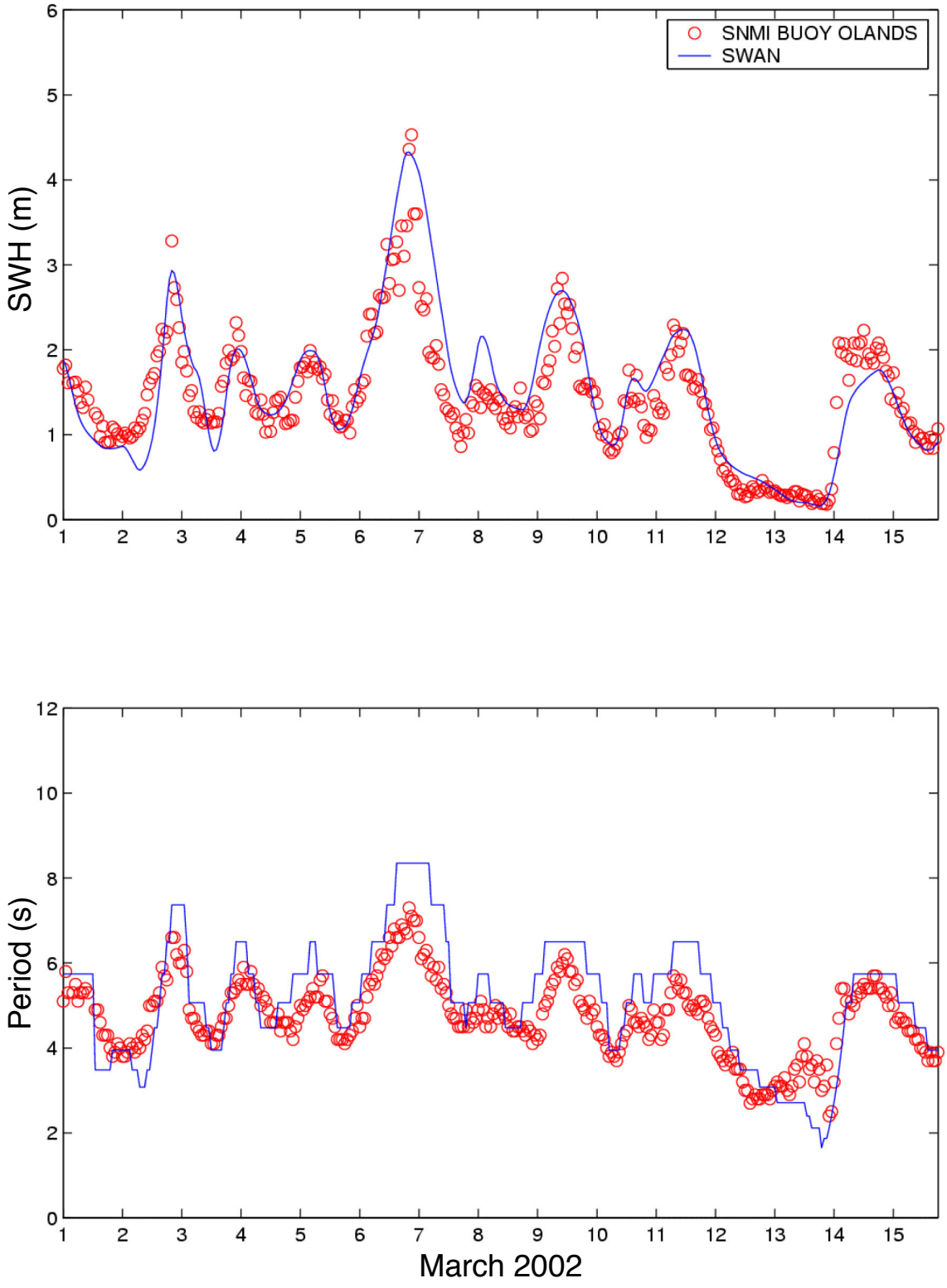

Fig. 30 — Results of comparison of SNMI buoy to SWAN model for (top) significant wave height (SWH) and (bottom) wave period for Test 7: Oland, Sweden

3.8 Test 8: Refraction

3.8.1 Purpose

Test 8 was performed to validate depth-induced refraction. It was an academic test case with comparisons to SWAN based on the analytical solutions of C. C. Mei (1983).

3.8.2 Test Characteristics

In order to test refraction, an infinitely long plane beach with parallel depth contours was considered. The depth contours were parallel to the *x*-axis and to the water line. Monochromatic, long-crested waves were propagating from a water depth of 20 m towards the shore (see Fig. 31). The travel distance of the waves perpendicular to the depth contours from the upwave boundary to the water line was 4000 m (slope equal 1:200). Ambient currents and wind were absent. The incident wave height (H_i) and period (T_i) were 1 m and 10 s, respectively.

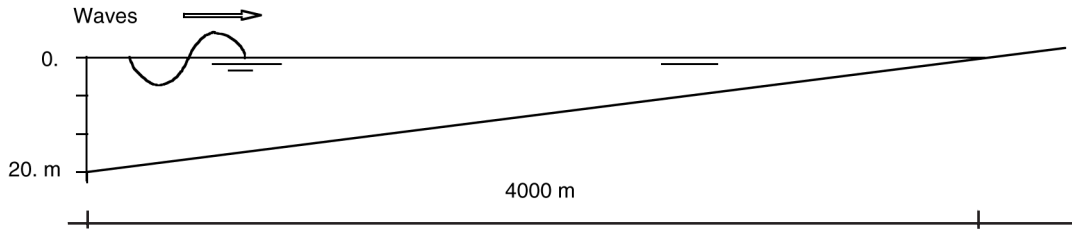

Fig. 31 — Refraction on an infinitely long plane beach (30 deg incident wave direction)

SWAN's 2-D mode was activated. The computational grid was oriented in the direction of the beach to prevent action from being shifted from one directional quadrant to another due to refraction (Holthuijsen 1993). From a uniform up-wave boundary, waves propagated at an angle of 120 deg to the depth contours at the boundary towards the beach. The wave field was characterized by a Gaussian-shaped spectrum and the directional distribution was equal to $\cos^{500}$. Output was generated along an output curve (from x = 10 km, y = 0 km, to x = 10 km, y = 4 km).

3.8.3 Analytical Solution

The significant wave height along an output curve, perpendicular to the depth contours, can be calculated by (see Mei 1983):

$$\frac{H^2}{H_i^2} = \frac{c_{g,i}}{c_g} \frac{\cos(\theta_i)}{\cos(\theta)},$$

where the wave direction θ can be calculated with Snell's law:

$$\frac{\sin\theta_i}{c_i} = \frac{\sin\theta}{c}.$$

3.8.4 Results

Figure 32 shows the model results in terms of SWH and mean wave direction and the analytical solution of Test 8.

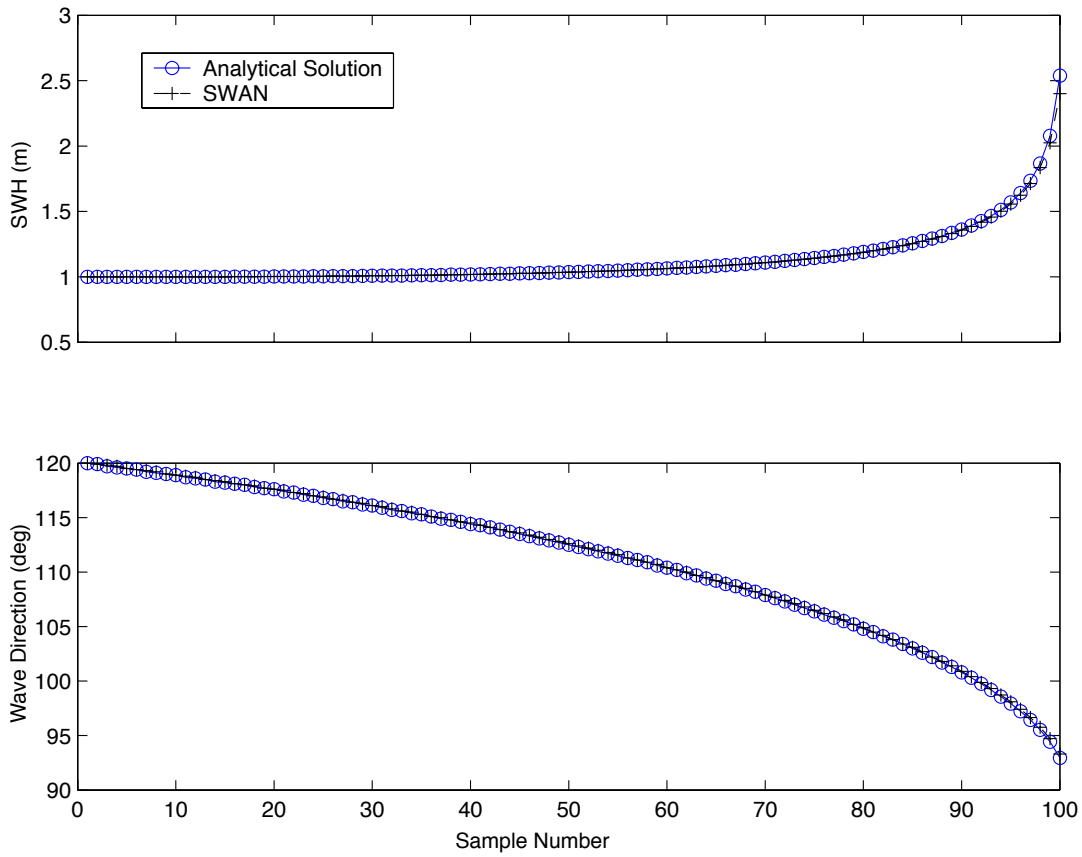

Fig. 32 — Model results for (top) SWH and the analytical solution for SWH and (bottom) mean wave direction and the analytical solution based on Snell's Law

3.9 Test 9: Currents (Slanting Current)

3.9.1 Purpose

The purpose of Test 9 was to validate wave propagation in the presence of currents (current-induced refraction and shoaling). The academic test cases for obliquely incident waves on the slanting current are based on the analytical solutions of Hedges (1987) and Jonsson (1993). The analytical solutions for the wave direction and the wave height, using Snell's law, $\sin\theta / c$ = constant, are

$$\theta = \arccos\left(\frac{gk_0\cos(\theta_0)}{[\omega - Uk_0\cos(\theta_0)]^2}\right)$$

$$H = H_0\sqrt{\frac{\sin(2\theta_0)}{\sin(2\theta)}}$$

3.9.2 Test Characteristics

A deep water region with uniform bathymetry, 4000 m long and infinitely wide, was considered. Essentially this was a 1-D test case. For all cases, monochromatic unidirectional waves propagate in the positive x-direction. The up-wave boundary was at $x = 0$. The incident wave height (H_i) and period (T_i) were 1 m and 10 s, respectively.

For Test 9, the wave direction at the up-wave boundary was 120 degrees. The current was parallel to the *x*-axis and positive in *x*-direction. The current velocity increased linearly from 0 to 2 m/s in the positive *x*-direction. Wind was absent and the water was infinitely deep.

3.9.3 Results

The computational results in terms of significant wave height and mean wave direction are shown in Fig. 33. The model results were compared with long-crested analytical solutions.

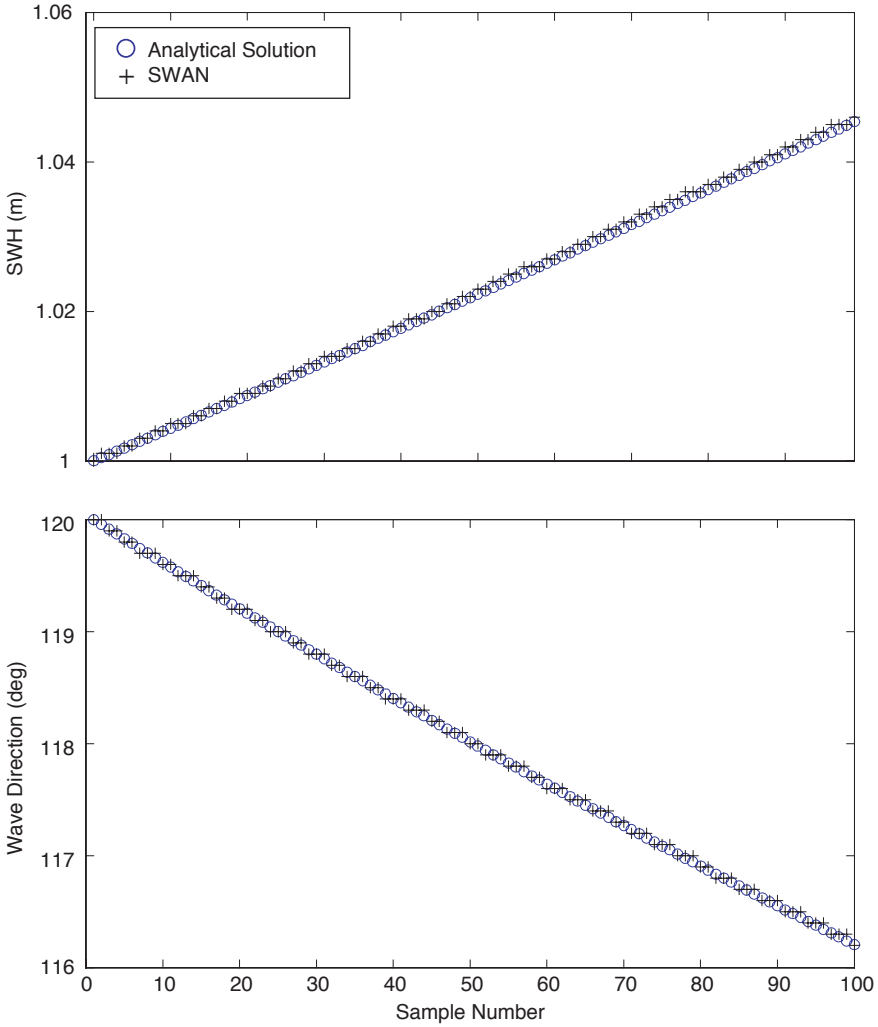

Fig. 33 — Model results for SWH and mean wave direction

4. CONCLUSIONS

This report summarizes previous and new validation efforts conducted for the third-generation wave model SWAN. The test cases documented in this report demonstrate that SWAN produces reasonably accurate results: given accurate forcing, wave height is usually well predicted, with no consistent bias. Mean period, however, does show a consistent negative bias, suggesting systematic overprediction of high frequencies and underprediction of low frequencies. Fortunately, this bias can be easily corrected/prevented without modification to the source code. With this modification, SWAN's ability to predict wave growth and decay is comparable to that of other third-generation wave models (and unlike other third-generation wave models, SWAN is suitable for application at any resolution and water depth).

SWAN was tested with the following features:

- nonstationary and stationary modes,
- currents,
- water levels,
- initializing with WAM directional wave spectra,
- initializing with buoy spectra,
- using Fleet Numerical Meteorology and Oceanography Center (FNMOC) operational wind products (e.g., COAMPS™), and
- using buoy-derived wind forcing.

Additionally, the test cases include running SWAN on both spherical and Cartesian grids, two analytical tests, and running SWAN in coastal areas, lakes, and larger regional domains.

The 40.11 release of SWAN is not intended to replace WAM (see below). SWAN is a third-generation wave model (as is WAM Cycle 4) and uses similar formulations for the source terms and some additional formulations, especially for shallow water. SWAN can be run to compute waves on scales much larger than coastal scales. SWAN accomplishes this by using a more accurate numerical propagation scheme in this latest release of the model. SWAN can perform calculations in spherical coordinates (the Steady State Wave Model (STWAVE) can not) allowing calculations in laboratory situations, coastal regions, shelf seas, and oceans, but not harbors since diffraction is not included in SWAN. The OpenMP release of SWAN will allow SWAN to run much faster (depending on the number of processors) on shared memory machines. SWAN has been tested on the NAVOCEANO IBM SP4 (marcellus) where it runs on up to 8 "threads," greatly reducing wall clock time.

4.1 WAM vs SWAN

Although SWAN is not intended to replace WAM, there are some nonstationary cases for which SWAN would be a more appropriate choice. While WAM can become unstable when run with irregular bathymetry, SWAN doesn't have such a problem. From a computational perspective, if the WAM resolution is less than ~10 km, it may be more cost-effective to run the OpenMP version of SWAN. At higher resolutions, SWAN's advantage in efficiency becomes much more apparent. Thus, SWAN could replace many of the implementations of the regional WAM run operationally at NAVOCEANO. The OpenMP SWAN has been tested on a multitude of platforms including SGI, COMPAQ, IBM SP, SUN SPARC, and LINUX systems. WAVEWATCH-III is another model that may be considered as a future replacement for WAM. This model has stability/robustness characteristics comparable to those of WAM.

4.2 SWAN vs STWAVE

Stationary modes for wave models can be used when the travel time of waves through the region is small compared to the time scale of the geophysical conditions such as wave boundary conditions, winds, and tides. While SWAN can be run in a nonstationary or stationary mode, the STWAVE model (Smith et al. 2001) can only be run in a stationary mode. SWAN is a full-plane model resolving waves propagating from any direction. STWAVE is a half-plane model and can require multiple grids being set up to address waves traveling from different directions. SWAN allows variable directional wave spectra (from models such as WAM and WAVEWATCH-III) to be placed along all its open boundaries to be used as a lateral boundary condition. STWAVE only assumes homogeneous boundary conditions, on a user-specified offshore boundary. Additionally, SWAN permits a user to specify a horizontally and time-varying wind field, while STWAVE specifies a uniform wind for a given time. Unlike STWAVE, SWAN can also be run in spherical and curvilinear coordinates. Overall, SWAN's capabilities are superior to STWAVE. Table 13 compares some of the

Table 13 — Comparison of Model Features

Model Features	SWAN	STWAVE
Wave propagation from any direction	YES	NO
Variable boundary condition	YES	NO
Diffraction	NO	YES[1]
Wind field can vary spatially over model grid	YES	NO
Refraction	YES	YES
Cartesian coordinates	YES	YES
Spherical coordinates	YES	NO
Curvilinear coordinates	YES	NO
Can be run in nonstationary mode	YES	NO

[1]STWAVE includes diffraction in a simple manner by smoothing wave energy. This process is grid-spacing dependent.

more important features contained in these models. In applications where the additional features of SWAN are not relevant or not necessary, one can expect that the accuracy of the two models will be comparable, but with STWAVE having a shorter run-time than serial SWAN.

4.3 1-D Stationary

SWAN can be run in a 1-D stationary mode for which there is no variation in the *y*-direction (the alongshore axis, typically) with forcing, input or output. In this manner, a constant slope can be specified for the input bathymetry. This setup would be similar to the 1-D Navy Standard Surf Model (NSSM). However, the NSSM output includes a parameterization for breaker type (spilling, plunging, surging), calculation for Modified Surf Index, surf zone width, and longshore current, outputs that are not available from SWAN.

5. ACKNOWLEDGMENTS

The authors wish to thank Dr. Y. Larry Hsu, Dr. Jim Kaihatu, and James Dykes at NRL for their insight and thoughtful discussion concerning the model.

GLOSSARY

CMAN	Coastal Marine Automated Network
COAMPS	Coupled Ocean Atmospheric Mesoscale Prediction System
DOD	Department of Defense
FNMOC	Fleet Numerical Meteorology and Oceanography Center
FRF	Field Research Facility
JONSWAP	JOint North Sea WAve Project
NATO	North Atlantic Treaty Organization
NAVOCEANO	Naval Oceanographic Office

NDBC	National Data Buoy Center
NGLI	Northern Gulf of Mexico Littoral Initiative
NOAA	National Oceanic and Atmospheric Administration
NOGAPS	Navy Operational Global Atmospheric Prediction System
NRL	Naval Research Laboratory
NSSM	Navy Standard Surf Model
ONR	Office of Naval Research
PET	Programming Environment and Training
RMS	Root Mean Square
RMSE	Root Mean Square Error
STWAVE	Steady State Wave Model
SWAN	Simulating WAves Nearshore
SWH	Significant Wave Height
UTC	Universal Time Coordinated
VTR	Validation Test Report
WAM	WAve Model
WAQUA	Water Quality/Circulation Simulation Model
WAVEC	Directional wave buoy from DATAWELL
WAVEWATCH-III	Full-spectral third-generation wind-wave model

REFERENCES

Booij, N., R.C. Ris, and L.H. Holthuijsen (1999). "A Third-Generation Wave Model for Coastal Region: 1. Model Description and Validation," *J. Geophys. Res.* **104**(C4), 7649-7666.

Collins, J.I. (1972). "Prediction of Shallow Water Spectra," *J. Geophys. Res.* **77,** 2693-2707.

Hedges, T.S. (1987). "Combination of Waves and Currents: an Introduction," *Proc. Instn. Civ. Engrs.*, Part 1, **82**, 567-585.

Holthuijsen, L.H., N. Booij, and R.C. Ris (1993). "A Spectral Wave Model for the Coastal Zone," *Proc. 2nd Internat. Sympos. Ocean Wave Measurement and Analysis*, New Orleans, 630-641.

Hwang, P.A., D.W. Wang, E.J. Walsh, W.B. Krabill, and R.N. Swift (2000). "Airborne Measurements of the Wave Number Spectra of Ocean Surface Waves. Part 1. Spectral Slope and Dimensionless Spectral Coefficient," *J. Phys. Oceanogr.* **30**, 2753-2767.

Jonsson, I.G. (1993). "Wave Current Interactions," in *The Sea*, *Ocean Eng. Sci. Ser.* **9**, (A), B. Le mehaute and D.M. Hanes, eds. (John Wiley, New York) pp. 65-70.

JONSWAP Group (1973). "Measurements of Wind-Wave Growth and Swell Decay During the Joint North Sea Wave Project (JONSWAP)," *Deut. Hydrogr. Z.,* A12.

Les, B.A.J. (1996). "Flow Computations in the Friesche Zeegat," M.Sc. Thesis, Delft University of Technology, Dept. of Civ. Eng., Delft, Netherlands.

Madsen, O.S., Y.-K. Poon, and H.C. Graber (1988). "Spectral Wave Attenuation by Bottom Friction: Theory," *Proc. 21st Int. Conf. Coastal Engineering, ASCE*, 492-504.

Mei, C.C. (1983). *The Applied Dynamics of Ocean Surface Waves* (Wiley, New York), p. 740.

Padilla-Hernandez, R. and J. Monbaliu (2001). "Energy Balance of Wind Waves as a Function of the Bottom Friction Formulation," *Coastal Eng*. **43**, 131-148.

Ris, R.C., N. Booij, and L.H. Holthuijsen (1999). "A Third-Generation Wave Model for Coastal Region, Part II: Verification," *J. Geophys. Res*. **104(**C4), 7667-7681.

Ris, R.C. (1997). "Spectral Modeling of Wind Waves in Coastal Areas," Ph.D. Thesis, Delft University of Technology, the Netherlands.

Rogers, W.E., P.A. Hwang, and D.W. Wang (2003). "Investigation of Wave Growth and Decay in the SWAN Model: Three Regional-Scale Applications," *J. Phys. Oceanogr.* **33**, 366-389.

Rogers, W.E., P. A. Hwang, D.W. Wang, and J.M. Kaihatu (2000). "Analysis of SWAN Model with In-situ and Remotely Sensed Data from SandyDuck '97," *Proc. 27th International Conference on Coastal Engineering,* Sydney, Australia.

Smith, J.M., A.R. Sherlock, and D.T. Resio (2001). "STWAVE: Steady-State Spectral Wave Model User's Manual for STWAVE, Version 3.0," Coastal and Hydraulics Laboratory, ERDC/CHL SR-01-1.

Stelling, G.S., A.K. Wiersma, and J.B.T.M. Willemse (1986). "Practical Aspects of Accurate Tidal Computations," *J. Hydrol. Eng*. **112**(9), 802-817.

Wakeham, D., R. Allard, J. Christiansen, T. Taxon, and S. Williams (2002). "The Distributed Integrated Ocean Prediction System (DIOPS)," Seventh International Workshop on Wave Hindcasting and Forecasting, Banff, Canada, Meteorological Services of Canada, 438-444.

Weber, S.L. (1991). "Bottom Friction for Wind Sea and Swell in Extreme Depth-Limited Situations," *J. Phys. Oceanogr*. **21**, 149-172.